



Conceptual Design of a Small Sample High Field RF Test Station for the Study of Superconducting RF Materials

P. Bauer, K. Ewald, T. Khabiboulline, T. Peterson

Fermilab, Technical Division

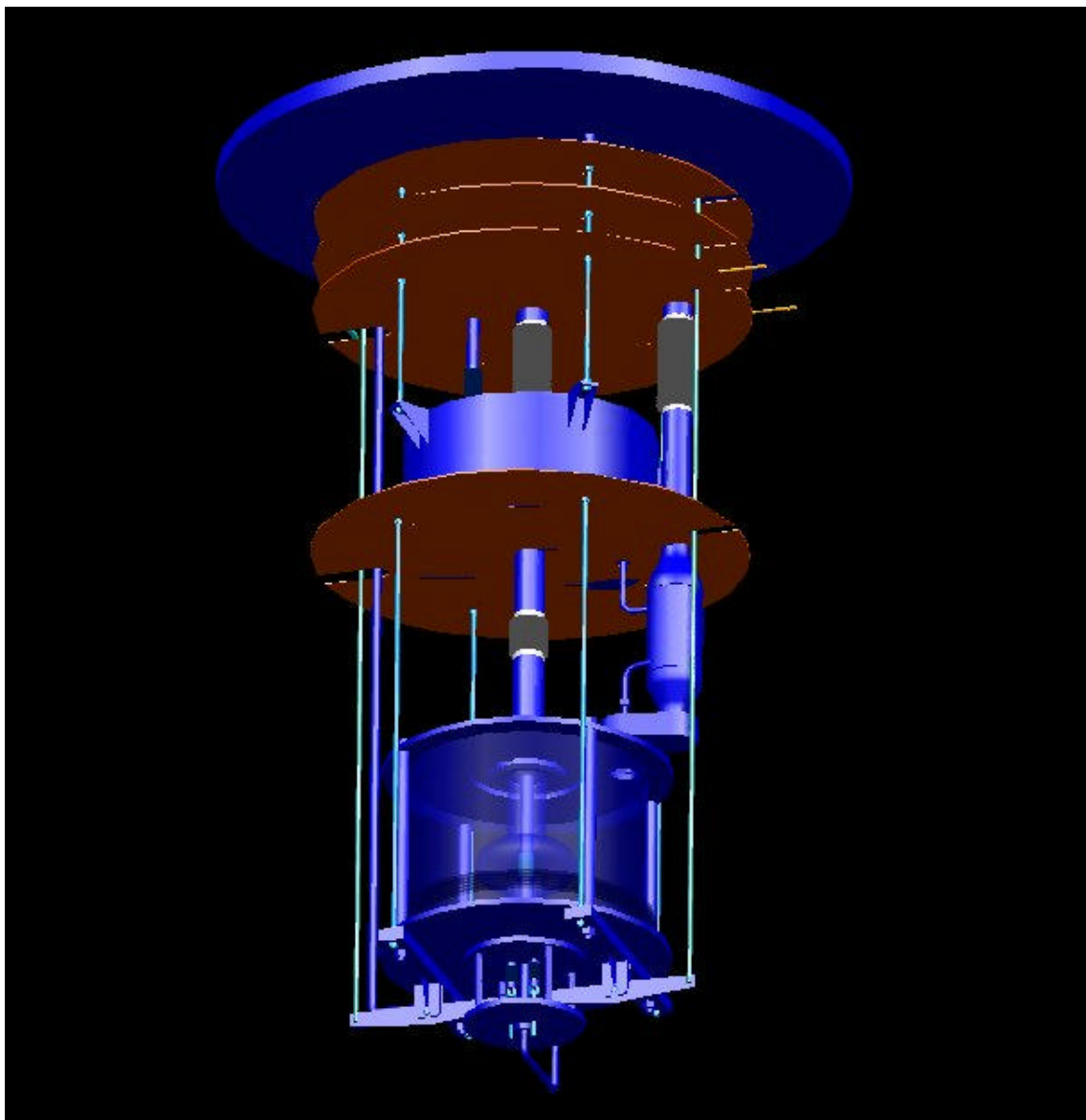
The following describes a possible design for a high-field, small sample RF test facility, which measures the RF surface resistance and the breakdown magnetic RF fields of small, cm² sized samples of superconducting materials for RF applications. The small sample measurement would be an essential tool in the ongoing quest for high gradients in the field of superconducting RF for particle accelerators. It can also be used to investigate and support the development of other RF materials, such as Nb₃Sn, with the potential to exceed the gradients achievable in bulk Niobium cavities.

The development of such a small sample, high field test facility is a challenging task. The design concept of the test facility presented here addresses all the major components of the measurement system, such as the cryo-system, the RF system and the measurement technique at a feasibility study level. Technical solutions for all of the issues are presented. A low risk strategy for the implementation of the test facility is also described and a preliminary cost-estimate given.

This design specification is a follow-up document to the original proposal of the small sample test idea, which was published under the title "Superconducting RF Material R&D at Fermilab". The scientific rationale for this activity is discussed further there.

Table of Contents

1) INTRODUCTION	4
1.1) The Sample-in-Host-Cavity Concept	4
1.2) Basic Specifications	5
1.3) The Cryo-System	6
1.4) The Sample-Holder	7
1.5) The RF-System	8
1.6) The Vacuum-Systems	8
1.7) The Measurement Technique	9
1.8) Other Issues	10
2) THE HOST CAVITY ASSEMBLY	11
2.1) Host Cavity Parameters	11
2.2) Host Cavity Assembly	11
2.3) Plots	12
3) THE HOST CAVITY RF FIELDS	16
3.1) Summary Field-Calculations	16
3.2) Peak Magnetic Fields	16
3.3) Peak Electric Fields	17
3.4) Parasitic Modes	17
3.5) Field Enhancement	17
3.6) Thermal Model	18
3.7) Plots	19
4) CRYO-SYSTEM	24
4.1) Basic Cryo-System Layout	24
4.2) Dewar Design	24
4.3) Host Cavity Cooling System	25
4.4) Sample Cooling System	26
4.5) Miscellaneous Systems	27
4.6) Plots	28
5) SYSTEM ASSEMBLY PROCEDURE	29
6) RF - SYSTEM	32
6.1) RF Power Requirements	32
6.2) RF System Design Outline	32
6.3) RF Measurement System	32
7) SAMPLE-HOLDER and SAMPLE-TRANSFER STAGE	34
7.1) Sample-Holder Design	34
7.2) Sample and Sample Instrumentation	35
7.3) Sample Exchange Procedure	35
8) MEASUREMENT TECHNIQUE	37
8.1) Q Perturbation Method	37
8.2) Thermometric Method	39
8.3) Quench Field Measurement	39
9) SAPPHIRE COLD BORE	39
10) MAGNETIC SHIELDING	40
11) VARIABLE COUPLERS	41
12) RADIATION SHIELDING	43
13) STEP-BY-STEP APPROACH	44
14) COST ESTIMATE	45
APPENDIX A	47
APPENDIX B	50
APPENDIX C	51



Model of the insert of the Small Sample High Field Superconducting RF test station. The insert hangs from the cryostat top-plate and consists of the host cavity cryostat (lower vessel), the LHe reservoir (upper-vessel) and the sample vacuum chamber (central column). Also shown is the cavity (inside the lower cryostat) with the sample, the variable drive system for the couplers, the 2 K pumping chimney. Not shown are the outer cryostat, the magnetic shield, the sample exchange chamber and sample transfer stage as well as the radiation shield and the RF power supply and control/measurement system hardware.

1) INTRODUCTION

1.1) The Sample-in-Host-Cavity Concept

The following lays out a possible design for a novel experimental apparatus that allows measurement of the RF surface resistance and the limiting RF fields in small samples of superconducting RF material. The measurement system consists of a

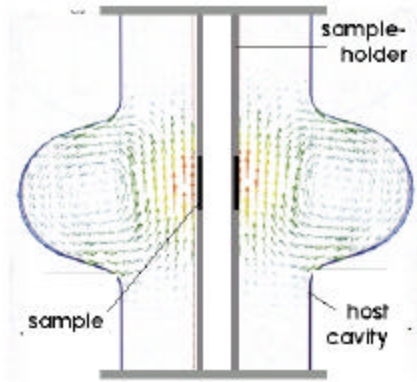


Figure 1: Magnetic field vectors in TESLA single cell cavity excited in TE010 mode with sample mounted on an axial rod in its center.

superconducting Nb single cell TESLA cavity, possibly supplied by DESY¹, which is used as a host resonator into which a small sample of superconducting RF material is introduced. The sample is a short cylindrical tube with ~30 mm outer diameter and ~50 mm long, which forms the mid-section of a Nb-tube (or sample-holder) that runs all along the center axis of the host cavity. The host cavity including the central tube is operated in a TE010 mode. In this mode the magnetic field is highest in and oriented along the cavity axis and thus concentrated at and parallel to the surface of the sample. The TE010 mode is also characterized by the fact that the electric field is low on all surfaces. Fig. 1 shows the calculated magnetic field distribution in a TESLA single cell cavity excited in the TE010 mode with a Nb tube along the center axis. The

TE010 mode frequency is 2.635 GHz, approximately twice the frequency of the TESLA accelerating mode. The magnetic field enhancement-factor, which is the ratio of sample magnetic field to the host cavity peak field, is ~2. The peak-field region in the cavity is located at the iris. Section 2 of this document describes in further detail the assembly of the sample in host cavity system. Chapter 3 discusses in detail the electromagnetic simulations.

Although not the first of its kind, this proposal's particular strength stems from the use of a TESLA single cell cavity as host for the sample. The very successful TESLA cavity R&D program has produced many single-cell prototypes that reached surface magnetic fields of up to 180 mT with low surface resistance. The use of a high performance TESLA single-cell cavity offers the historic opportunity to increase the host cavity performance by an order of magnitude with respect to former trials. Complemented by a modest magnetic enhancement factor of 2, magnetic fields of up to 360 mT can be achieved on the sample. This should be sufficient to explore the quench fields of all known superconducting materials currently employed or with potential for superconducting RF application such as Nb, Nb₃Sn and NbN. Stretching of the TESLA-type cavity can potentially yield further magnetic field enhancement of up to 3.5. It is important to note, however, that, as a result of the higher operating frequency as well as high surface magnetic fields the surface resistance is large, causing significant surface RF heating. For that reason the system needs to be operated in a pulsed mode with a high power klystron.

¹ DESY indicated that a TESLA single cell cavity could be made available for this purpose – e-mail, D. Proch (DESY), L. Lilje (DESY) and H. Edwards (FNAL), Aug. 13th, 2003.

1.2) Basic Specifications

Fig. 2a shows a sketch of the conceptual design of the facility needed to implement the sample in host cavity idea. The major sub-components of the small sample test facility are: the host cavity and sample cryo-systems, the sample-holder and sample vacuum system, the RF power supply system and the surface resistance measurement instrumentation. Possible technical solutions for these subsystems are described in detail in this document. Their design aims at satisfying the main specifications of the test-facility, which are:

- that the host cavity can be reliably and efficiently operated at $1.5\text{--}2\text{ K}$, at a quality factor of $Q_0 \sim 10^{10}$ up to peak magnetic fields of $\sim 180\text{ mT}$;
- that the sample can be exchanged without removing and warming of the host cavity and that its temperature can be regulated independently from the host cavity in the range of $1.5\text{--}20\text{ K}$;
- that the RF surface resistance and quench field of the sample can be measured in the GHz -range with a 1% accuracy in the full magnetic field range $0\text{--}500\text{ mT}$.

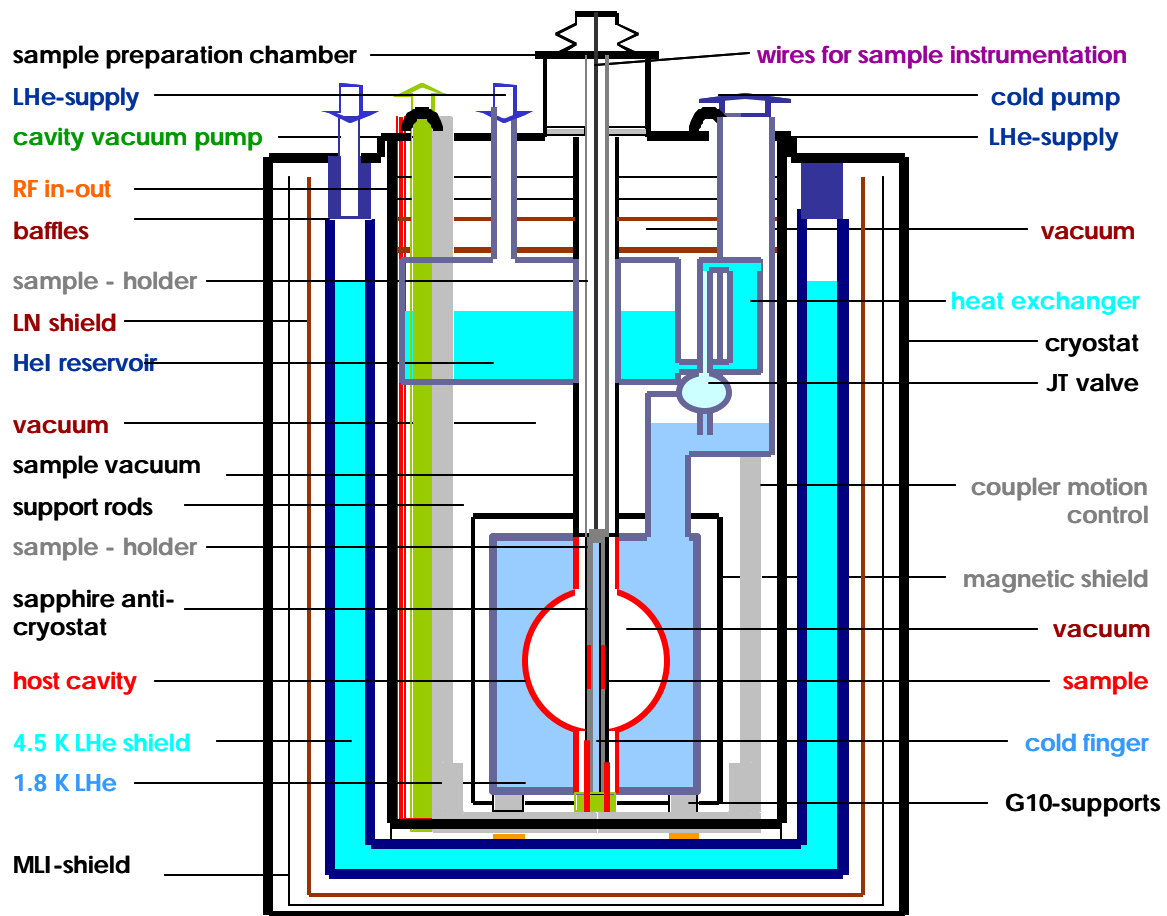


Figure 2a: Sketch of short sample, high field RF test facility. Note that the upper portion of the cryostat (shield section and sample exchange chamber) is compressed in this schematic.

A major design goal of the small sample, high field RF test facility is that it allows for fast turn-around and therefore for frequent sample exchange. This is only possible if the vacuum- and cryo-systems of the host cavity and sample are separated. To separate the host cavity vacuum system from the sample vacuum system we propose to use a thin-walled sapphire tube, which is placed along the axis in the center of the host cavity to contain the sample and sample-holder. The sapphire tube fulfills the role of a cold bore, separating the host cavity vacuum on its outside from the sample vacuum on its inside and thus protects the inside of the host cavity from contamination during the sample exchange. There are issues related to RF heating and field emission in and from the sapphire. Therefore the facility is designed such that the sapphire bore can also be removed if it cannot be made to work. Since the exchange of the sample is performed in air a special process was developed to reduce the contamination of the sample vacuum system (which includes the sapphire bore). This process includes the use of a gate valve to separate the sample exchange chamber from the sapphire bore during sample exchange and the presence of a strong flow of filtered nitrogen in the sample chamber during sample exchange. These and more issues are discussed in section 7.

It was previously thought that this facility could be operated in the low power mode with a traveling wave type amplifier. One of the results of the design study presented here is that a high power klystron-type supply was found to be necessary to drive the host cavity in a fast pulse mode. The pulse duration needs to be limited to less than 1 msec (100 microsecs) at sample peak fields of 200 mT (500 mT) to prevent significant surface heating on the sample (and the host cavity) as a result of the high operating frequency as well as high surface magnetic fields. Section 6 is describing the RF power system needs in detail. Section 4 presents the results of thermal calculations that motivate the need for fast-pulsed measurements. Chapter 13 presents possible alternatives to the high power, short pulse approach. The feasibility of these solutions needing to be demonstrated, they were not adopted as the baseline for this conceptual design study.

1.3) The Cryo-System

The cryo-system we propose combines standard technology for the cooling of the host cavity to its operating temperature (1.5-2 K) and a novel approach for the sample cooling.

The host cavity is cooled by a 1.5-2 K bath, which is supplied with liquid helium from a 5 K reservoir, pre-cooled in heat exchanger and expanded through a Joule-Thompson (JT) valve. In addition the host cavity bath is pumped to lower the temperature further via reduction of the vapor pressure. The cryo-system is designed for low loss operation of the host cavity, such that it can be kept cold over extended periods, while the samples are replaced on a daily basis. As can be seen in Figure 2a, this is achieved by surrounding the 2 K system with 4π coverage 5 and 90 K shields. The results of calculations of the expected static and dynamic heat loads in the host cavity bath are given in section 4.

The sample is cooled indirectly by a cold finger placed in the center of the host cavity, which in turn is supplied by the 2 K bath. The cold finger consists of a 10 mm inner diameter Cu tube, closed at the top and supplied from the bottom with superfluid helium from the host cavity bath. It slides into the sapphire bore, leaving

a gap for the sample. The sample is cooled by conduction from the cold finger through flexible copper springs, attached to the outside of the cold finger. It is important that the liquid level in the 2 K bath is higher than the top of the cold finger to prevent the formation of gas at the top of the cold-finger during the RF pulse. The detailed description of the cryo-system in section 4 includes a discussion of the results of calculations of the maximum peak heat load as a function of liquid overhead. The advantage of the indirect sample cooling scheme is that it simplifies the regulation of the sample temperature using heaters mounted on the inside of the sample. It also ensures that the sample is in adiabatic conditions during the short RF pulse, simplifying the derivation of the surface resistance from the sample temperature rise.

1.4) The Sample-Holder

The section of the sample-holder within the host cavity (Fig. 2b) consists of a ~30 mm OD Nb tube, made of two sections, top and bottom, which can be unscrewed from each other and with the sample wedged in between. The sample is indirectly cooled by conduction from the cold finger through flexible copper springs attached to the cold finger. The outside surface of the sample-holder tube has to be carefully surface treated, since it is exposed to the RF fields. The 50 mm sample is long enough to move the gaps between the sample and the upper and lower portions

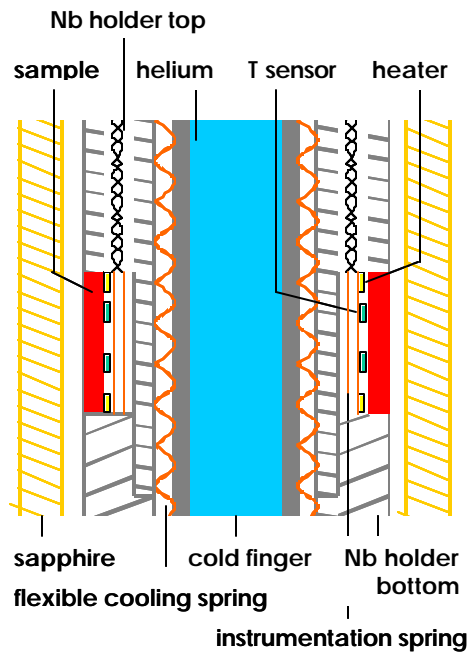


Figure 2b: Detail of sample-holder in the mid-cavity section where the sample is placed.

of the sample-holder out of the high field region. The shielding currents in the sample run azimuthally, and therefore parallel to the gap, which should therefore not impact the performance. There is, however, field enhancement, which occurs at the edges of the sample-holder and sample on each side of the gap. The design goal is to achieve a 15% magnetic field margin at the sample-edge (i.e. the field at the sample edges should be 15% smaller than the peak field in the middle). More on this issue can be found in chapter 3. Temperature sensors and heaters are mounted on a stainless steel foil on the backside of the sample, which acts as a spring and pushes the sensors against the sample. The sensor wires run upwards within a channel in the wall of the sample-holder Nb tube. The instrumentation is thus built into the sample-holder and not the sample, simplifying the sample assembly and exchange. The part of the sample-holder between the cryostat top and the host cavity is made of stainless steel to limit heat influx from the room temperature region at the top. Its diameter is larger than that of the bottom Nb portion within the host cavity so that the sample is protected from mechanical damage during insertion or removal of the sample-holder from the sample vacuum channel. Also, it is pre-cooled at 90 K and 5 K in

thermal intercept stages to reduce the influx of heat from the top, which is at room temperature.

1.5) The RF-System

The RF system supplies power to the cavity. The power supplied to the RF cavity needs to be sufficient to overcome wall loss in the resonator and transmission loss as well as include some overhead. Most importantly, however, it was found during the preliminary technical analysis presented here, that the surface resistance measurement needs to be performed in the pulsed mode, requiring cavity fill times as short as 10^{-5} secs. To supply the stored energy of ~ 2 J in ~ 100 microsec ~ 40 kW of power are required. Only a klystron can supply this power at ~ 2.6 GHz. The sharpness of the resonance in superconducting cavities requires the use of a feedback loop to maintain the resonance condition in the drive circuit in the presence of microphonics and Lorentz-force detuning.

To limit the RF power requirement and to reach the specified measurement accuracy it is necessary to achieve a Q of 10^{10} in the host cavity. This goal has been surpassed at DESY in special tests in which TESLA single cell cavities were tested in the same TE010 mode at peak magnetic fields of up to 120 mT^2 . It has not yet been achieved, however, in a setup that includes a central Nb rod (sample-holder). It was found at DESY that all parts exposed to RF fields, including the flanges, needed to be made of Nb or NbTi with a good surface finish. Given the challenges it is required that the high Q is first demonstrated in the host cavity with sample-rod assembly in a dedicated pre-cursor experiment (see discussion of the step-by-step plan in section 13).

The TE010 mode is coupled into the host cavity with a high power co-axial input coupler. An output coupler measures the cavity fields. Obviously the couplers need to be variable and made entirely from Nb. By pulsing the host cavity toward increasing surface magnetic fields on the sample, the surface resistance and the quench field of the sample can be measured. The measurement of the incident, reflected and transmitted power allows the setting of the variable couplers to the unity coupling condition required for the measurement of the cavity Q_0 . The attained field strength in the cavity is derived from the power dissipated in the cavity and the signal in the (calibrated) output coupler. Further details regarding the measurement technique are discussed in section 8.

1.6) The Vacuum-Systems

There are several separate vacuum systems: the test-station vacuum, the host cavity vacuum and the sample-vacuum system. The test station vacuum system comprises the cryostat vacuum shield, the 2 K pumping line vacuum and, most importantly, the volume into which the insert with the host cavity and sample is placed. It is thus a very large system requiring a large pumping capacity. The sample vacuum system consists of the long cylindrical volume bounded by the sapphire tube, the sample vacuum tube (which essentially extends the sapphire to

² D. Reschke / DESY, personal communication

the cryostat top plate) and the load lock chamber. The separation between the sample and host cavity vacuum systems, however, is artificial. To allow for differential thermal contraction effects (as well as prevent strong pressure differentials across the thin walled sapphire and allow its removal in case of field-emission problems) the sapphire bore is loosely assembled into the host cavity, thus creating a weak coupling between the two vacuum systems. The operational procedures for the test station should therefore account for this condition, and i.e. the pumping has to proceed always on both simultaneously.

The load-lock chamber is separated from the sample vacuum tube by a gate valve to prevent contamination during sample exchange, when the load-lock chamber is exposed to ambient. Although the load-lock chamber is pumped out before the gate valve is re-opened and the sample is introduced into the host cavity, there is a risk of contaminants falling into the sample vacuum tube. For that reason the sample exchange in the load lock should be performed under strong flow of dry and filtered nitrogen. Also, equipment required for in-situ thermal outgassing of the sample vacuum channel walls should be built into the system. Obviously the host cavity and sample vacuum systems have the most stringent specifications. They have to operate at 10^{-9} mbar or less.

1.7) The Measurement Technique

Precision measurement of the RF surface resistance of a superconducting sample is not a simple task. For that reason two parallel measurement strategies are pursued: the Q-perturbation method and the thermometric method. Both methods have been used successfully in the past.

The change of Q produced by a particular sample with respect to a reference sample is derived from changes in the field decay characteristic following a short RF pulse, as evidenced in the reflected power and the cavity pick-up signals. More precisely, the Q perturbation method consists in measuring with the pick-up the difference of the Q decay curve time constant following a pulsed excitation of the cavity between the case with a reference sample and with the sample. Since the time constant is proportional to the loaded Q of the cavity the measured reflected and incident powers also need to be taken into account to obtain the unloaded Q of the cavity. In the unity coupling condition, however, the unloaded Q is simply twice the loaded Q. If the surface resistance (at different fields) is known for the reference sample, the surface resistance of the sample can also be derived in absolute. The reference sample can be cut from the same material as used for the sample-holder and with a combination of electromagnetic modeling of the cavity fields and incident/reflected power measurements, the reference sample surface resistance can be known in absolute. Issues with this technique are the field (time) dependence of the decay time constant from which the loaded Q is derived as well as perturbative high field phenomena such as field emission. Also the pick-up needs to be calibrated. There is, however, an alternate method, which consists in determining the surface resistance of a sample directly from the measured cavity field and dissipated power. This procedure, however, also requires the exact knowledge of the surface resistance of the cavity with the reference sample and a well-calibrated pick-up. In addition, as an alternate method, it is proposed to measure the sample surface resistance using the thermometric method.

The thermometric method derives the surface resistance from the temperature rise of the sample during the RF pulse. The measurement of surface resistance at the $n\Omega$ level requires temperature measurement with mK precision. Note, however, that the “typical” surface RF dissipation (at a surface magnetic field of 200 mT and a surface resistance of 100 $n\Omega$) on the sample is 6 W (assuming a constant field over the entire sample surface). Assuming a 31 mm OD, 50 mm height and 2 mm thick sample, a temperature rise of 600 mK/msec (not counting the increase of the surface resistance due to the increase in temperature and assuming a specific heat of 1 kJ/K/m^3) is expected. Therefore, to prevent thermal run-away due to RF heating, both approaches require a fast pulsing technique.

1.8) Other Issues

Additional issues addressed in this conceptual design report are:

- Magnetic shielding of the host cavity to a level of $<1 \text{ mT}$ or better (as achieved in the existing TESLA prototype cryo-modules) is necessary (section 11).
- Given the large number of vacuum systems (host cavity, cryostat and sample) and the cryogenic circuit, all of which are connected to strong pumps, a careful control and mitigation of vibration is required.
- Given the possibility of measurements in the accelerating mode, integrated accelerating voltages of up to 5 MV are to be expected. Radiation shielding of the facility during operation is therefore required. The facility should be installed in a pit and the top plate covered with a shielding dome. The goal is to reduce the worst-case radiation level outside the shield to 0.1 mrem/hr or less (section 12).
- To optimize Q , variable couplers are required. The current design foresees that all its components are made of Nb and that they are brought into the host cavity from underneath with an orientation parallel to the cavity axis. The design-stroke of the couplers is 1". Further discussion of the coupler can be found in chapter 12.
- A step-by-step approach is proposed for the implementation of the test system in order to minimize the risk of failure. As a first step a rod-in-cavity test (without sapphire is proposed). Such a test should demonstrate that a Q of 10^{10} can be achieved in a TESLA single-cell cavity, equipped with a central rod and operated in the TE010 mode. Further details of the step-by-step approach are discussed in section 13.
- Fermilab's Technical division may get involved in RF measurements on high power input couplers and prototype cavities for CKM and the TTF-3rd harmonic cavities in the near future. Possible synergies with these RF measurement activities should be studied. E.g., if the cryostat is wide and deep enough it could also be used for that purpose and possibly costs could be shared. This also implies that the host cavity cryostat should be removable to make place for a different measurement system.

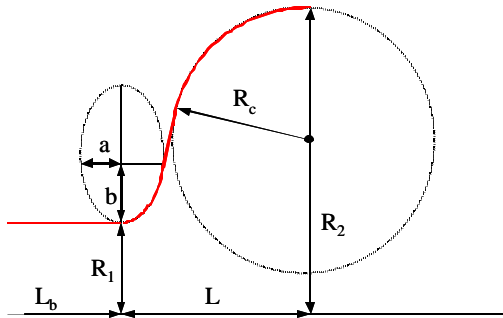
The following discusses the detailed design of the major sub-components of the small sample test facility as introduced above. In addition, a separate discussion of the issues regarding the most critical items of the facility, such as the sapphire bore, variable couplers and the magnetic shield, is given. Finally a step-by-step plan is proposed as a low-risk strategy to achieve the goal of building and operating this high power, small sample RF facility. A rough cost estimate is also provided (section 14).

2) THE HOST CAVITY ASSEMBLY

2.1) Host Cavity Parameters

The host cavity is assumed to be of the standard TESLA single cell cavity type. The host cavity geometry parameters are specified in Table 1. It includes NbTi flanges at both ends. The total length of the cavity is 392 mm, from one end of the beam tube to the other. The beam tubes extend ~1 mm beyond the end-flanges. The end-flanges have through-holes. To seal the holes NbTi adaptor flanges need to be bolted to the cavity end-flanges with Al gaskets as seals. Fig. 3 shows the host cavity assembly, including the sample-holder, the sapphire bore and the couplers. As a general rule all components exposed to RF fields (including the couplers) are made from Nb or NbTi. Furthermore all these parts should be outgassed at high temperature and their surfaces prepared with the same rigorous process that is applied to the inside surface of the cavities.

Table 1: Geometry parameters of standard TESLA one-cell cavity (end-cell). The dimensions given apply to the inside of the cavity. Also note that the beam-pipe extends 1 mm ("lip") beyond the cavity end-flange.



parameter	symbol	(mm)
Length	L	56
iris radius	R_1	39
cell mid-point radius	R_2	62.96
elliptic radius 1	a	10
elliptic radius 2	b	13.5
circular radius	R_c	40.34
beam pipe length	L_b	139+1

2.2) Host Cavity Assembly

The host cavity is assembled into the host cavity cryostat. The host cavity cryostat consists of stainless (Nitronic 40) bottom and top plates welded to a stainless (Nitronic 40) cylinder with a (welded) bellows section that allows the cryostat vessel to expand vertically and to adapt to changes of the host cavity length. Four tie rods made of Titanium, clamped to the top and bottom plates of the cryostat, stabilize the vessel and ensure that it shrinks at the same rate as the cavity during cool-down. The tie rods can be adjusted to the host cavity length with shims. The host cavity is attached to the cryostat at the top and bottom via the so-called cryostat flanges. They are complicated because they include ports for the sample, the pumping lines and the couplers. To prevent thermal contraction issues the cryostat top and bottom plates and the cryostat flanges are all made of stainless steel. The cryostat flanges are bolted from the outside into the so-called adaptor flanges. The adaptor flanges are made from NbTi because of their exposure to RF fields on the inside. Their purpose is to seal the host cavity and to shield the stainless cryostat flanges from the RF fields. The adaptor flanges need to provide a superfluid grade seal on both sides (to the cavity and cryostat flanges) with Al

gaskets. Note that the cavity should be assembled in a clean room. In addition, to prevent settling of dust, a constant flow of dry and filtered N_2 should be supplied to the cavity during assembly, either through the top while open or the pumping port at the bottom when closed. Fig. 3 shows the host cavity assembly together with the adaptor and the cryostat flanges.

The sapphire bore tube is contained within the adaptor flanges, which have specially prepared grooves. The sapphire bore is not firmly attached to the adaptor flanges. The groove in the top adaptor flange provides 1 mm additional vertical space to allow the sapphire tube to grow relative to the host cavity during cool-down (Sapphire has an integrated thermal shrinkage coefficient of 0.0003, 5 times less than Nb (0.0014)). This groove represents a weak coupling between the host cavity and the sample vacuum systems.

Fig. 4 shows a detailed view of the bottom end of the host cavity assembly. The bottom cryostat flange can be seen in detail. It includes the bolt and seal circles for the couplers as well as the vacuum pumping port and the cold finger guide-tube, which are both welded to it. The pumping port is a 20 mm diameter hole to which a short adaptor is welded that allows attaching the flexible pumping line. The coupler ports consist of two holes through which the coaxial couplers pass. The couplers can be moved further into the cavity or retracted with a mechanical system that is driven from outside the cryostat. The coupler assemblies are further described in section 12. The 14 mm outer diameter cold finger enters from underneath into the cold-finger guide-tube and is brought into position in the center of the host cavity. The vacuum seal is provided in the flange with which the cold finger tube is attached to the cold-finger guide-tube.

On the topside the cavity is attached to the cryostat via the top adaptor flange very much like on the bottom side. In the middle the top adaptor flange has a hole through which the sample-holder passes. The cryostat top flange has a conical taper on the topside against which the sample-holder rests. A temporary lid is installed to close this hole during assembly. Fig. 5 shows a detailed view of the top end of the host cavity assembly. The top cryostat flange also has the bolt-circle and gasket ring needed to attach the upper sample vacuum chamber tube.

Fig. 6 shows a zoom into the center section of the host cavity, where the sample is located. The sample and sample-holder are described in further detail in chapter 7. The sample-holder is centered along its entire length on the cold finger. On the topside the sample-holder is seated in the cone of the top adaptor flange. This closes a gap through which field leakage could occur. At the bottom end it rests on the bottom adaptor flange. Since the sample-holder, host cavity (and flanges) are made from Nb no differential thermal shrinkage issues are expected. The cold finger is made of Cu and will therefore shrink away from the sample-holder during cool-down. As discussed above the smaller thermal shrinkage of the sapphire bore is taken into account in the design of the top adaptor flange.

Additional issues are that all bolts used should be degreased using detergent in an ultra-sonic bath. To prevent galling they should be gold-plated.

2.3) Plots

Conceptual Design of a Small Sample High Field RF Test Station

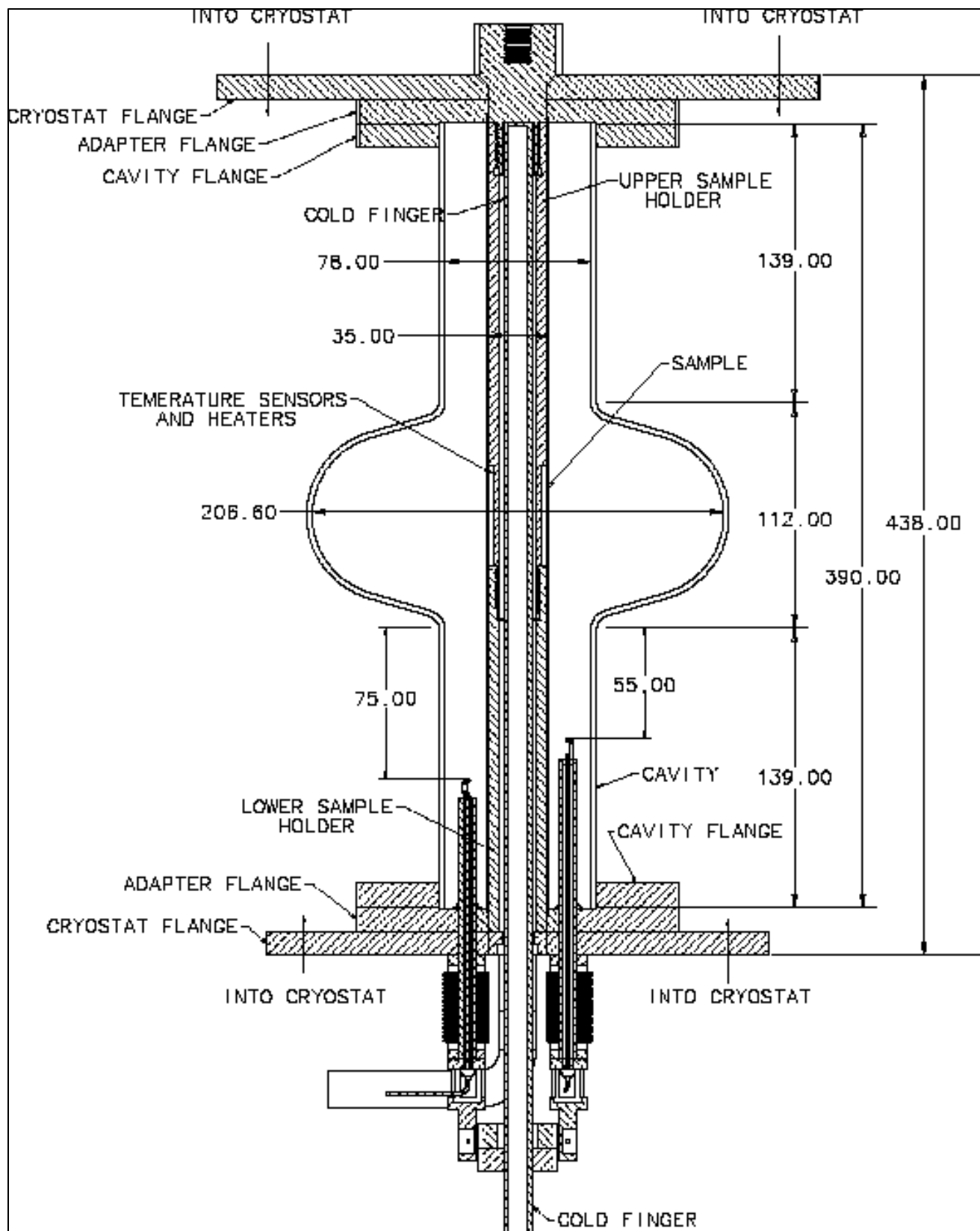


Figure 3: Host cavity assembly including sapphire bore, sample-holder, adaptor flanges, cryostat top and bottom flanges and input/output couplers (all measures in mm).

Conceptual Design of a Small Sample High Field RF Test Station

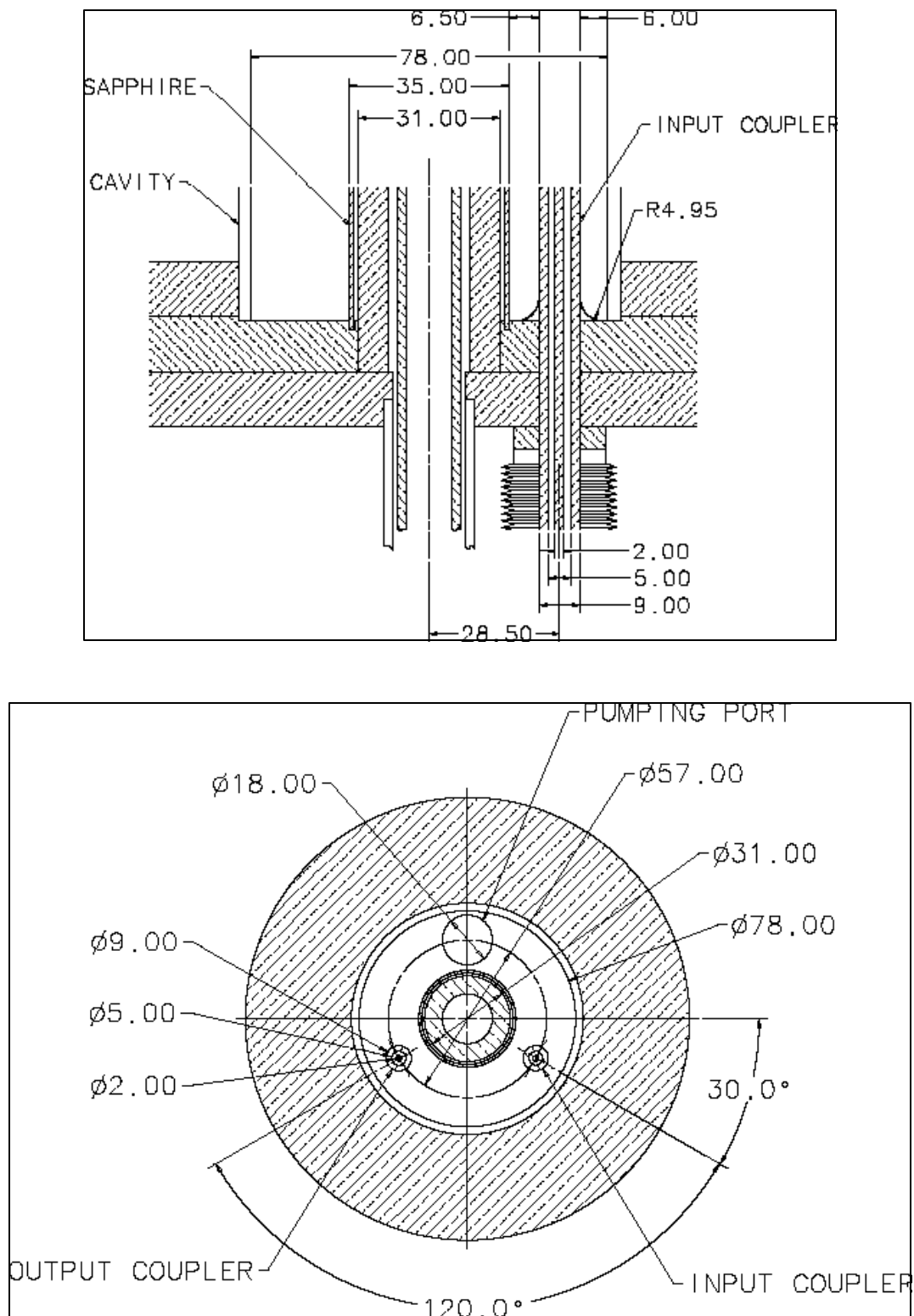


Figure 4: Host cavity assembly including sapphire bore, sample-holder, adaptor flanges, cryostat top and bottom flanges and input/output couplers. Zoom into bottom section (all measures in mm).

Conceptual Design of a Small Sample High Field RF Test Station

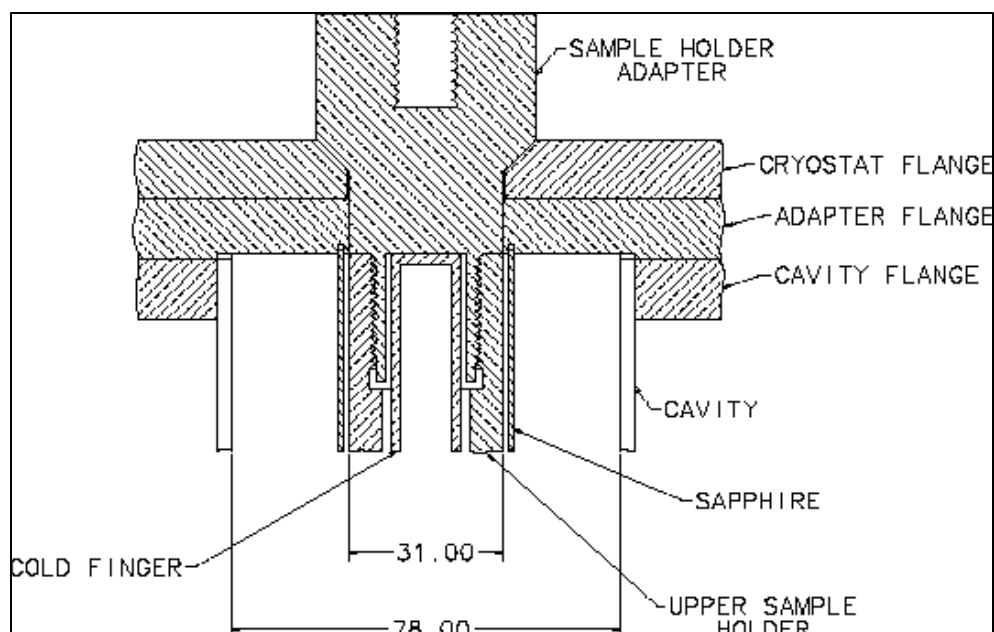


Figure 5: Host cavity assembly including sapphire bore, sample-holder, adaptor flanges, cryostat top and bottom flanges and input/output couplers. Zoom into top section (all measures in mm).

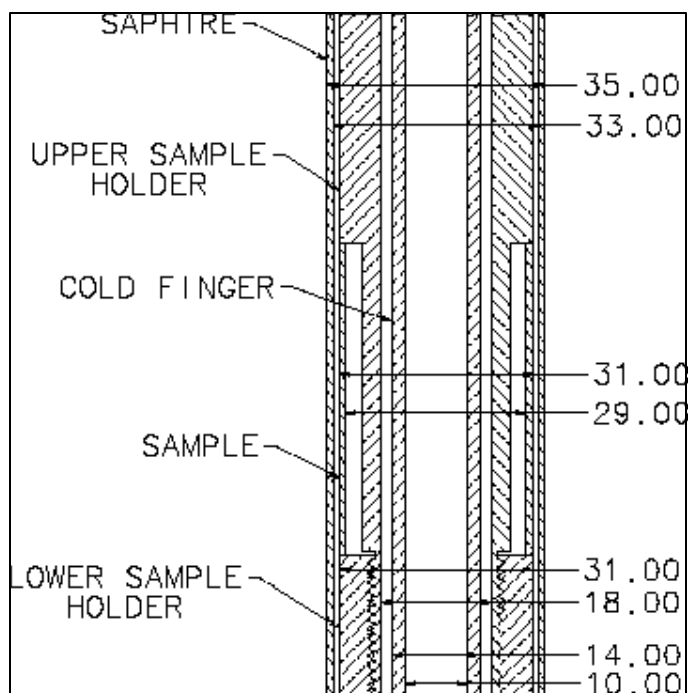


Figure 6: Host cavity assembly including sapphire bore, sample-holder, adaptor flanges, cryostat top and bottom flanges and input/output couplers. Zoom into middle section (all measures in mm).

3) THE HOST CAVITY RF FIELDS

3.1) Summary Field-Calculations

The RF field simulation presented in the following was performed with HFSS for the host cavity assembly, including flanges, sapphire bore, sample-holder and couplers as presented in chapter 2. Fig. 7 shows the HFSS model. The calculation assumed that all components that are exposed to RF fields are made from high purity Nb (or from NbTi) with a high field RF grade surface finish. Table 2 summarizes the main electro-magnetic properties of the small-sample in host cavity system.

Fig. 7 shows the calculated electric and magnetic field distribution for the 2.635 GHz TE₀₁₀ mode in a TESLA cavity with a 31 mm OD Nb sample-holder (containing the sample) along its center axis. The magnetic field is highest at the center of the sample and the field orientation is parallel to the sample surface. The highest surface magnetic field region on the host cavity is located half way between the iris and the equator.

The electric field is torroidal (see Fig. 7) and strongest in the middle between the cavity center and equator. The maximum surface electric field occurs at the host cavity iris. The fields are strongly attenuated in the cut-off tube.

Table 2: Magnetic and electric field characteristics in the small sample host cavity.

Frequency of the TE ₀₁₀ mode (GHz)	2.635
Sample magnetic field to cavity peak field ratio	1.9
Peak electric to peak magnetic field ratio (MV/m/mT)	0.255
Stored energy at 100 mT peak magnetic field (J)	2.1

3.2) Peak Magnetic Fields

Fig. 8 shows the magnetic field strength along a representative path through the host cavity as well as the sample and sample-holder. The ratio of surface magnetic field on the sample to the cavity surface is 1.9. Neglecting the gap effect, the magnetic field is reduced to 70% from the center of the sample to the edge of the sample (± 25 mm from center). Although the shielding currents in the sample run azimuthally, parallel to the gap, field enhancement occurs on the edges on both sides of the gap. With the worst-case edge geometry, with a circular edge, the peak-field at the edge is 15% below the peak field in the center of the sample.

Fig. 9 shows the magnetic field across the gap region for different edge shapes (or ellipticities). Round edges are worse (as bad as a sharp corner) and the field enhancement is independent of the edge radius (except that larger edge radii move the peak field point away from the gap). Elliptical edges have strongly reduced field enhancement. The sample and sample-holder edges bounding the gap implemented in the model used to obtain the field profile in Fig. 8 used the worst-case scenario with a circular 0.5 mm radius edge. The calculation also assumed that, except for the rounded edges there is no gap between the sample and the sample-holder. A gap would make the field enhancement issue worse. Although not pursued here, it is also possible to shape the sample such as to obtain a flat field profile.

3.3) Peak Electric Fields

Fig. 10 shows the calculated radial profile of the electric field across the cavity. The calculation assumed an $\epsilon=10$ in the sapphire. The peak-electric field to sample (peak) magnetic field ration is 0.255 MV/m/mT, i.e. at a peak surface magnetic field of 200 mT on the sample the peak electric field is 51 MV/m. The peak electric field on the sapphire tube outer surface is 10% of the peak field in the cavity (assuming a sapphire tube wall thickness of 1 mm and a tube OD of 35 mm). Therefore, at a 200 mT surface magnetic field on the sample, electric fields on the sapphire reach ~ 5 MV/m, very close to the break-down fields found in ceramic RF windows. Another concern is related to the RF heating in the sapphire as a result of high magnetic fields. With 0.085 % of the stored electric energy being concentrated in the sapphire, and a (worst-case) loss tangent of $\tan\delta=10^{-8}$ the RF heat load in the sapphire is 0.25 W for an RF pulse amplitude of 85 mT.

3.4) Parasitic Modes

The HFSS calculation of the S21 coupling factor between the input and output coupler reveals several near resonances. Table 3 lists the ones closest to the operating point for two different coupler positions. Note that in these calculations the in and output couplers were moved together and that the two positions analyzed are further toward the cavity center than the case shown in the assembly drawing in Fig. 3. In Fig. 3 the distance between coupler-loop tip and cavity center is 111 mm. The calculations were performed for the 100 and 90 mm cases. Examples are the two polarizations of the TM210 quadrupole mode close to 2.483 GHz. The resonances near 2.53 GHz correspond to coaxial modes TEM007. At 2.58 GHz and 2.66 GHz are other coaxial modes related to the antennas, so their frequency depends on the antenna length. The resonances near 2.804 GHz correspond to sextupole modes TE310 and its different polarizations. Fig. 11 shows S21 for two different coupler positions. Note that one particular resonance shifted from 2.579 GHz to 2.662 GHz when pushing the coupler from the 100 mm to the 90 mm case. This parasitic mode therefore crossed the operating frequency. It is necessary to be aware of this issue to prevent exciting this particular parasitic mode when adjusting the Q_{ext} of the couplers. Also, as a general rule it was found that the Q_{ext} of the antenna increases about 10 times when antenna length is decreased by 10 mm. Apart from this issue, however, it was found in both cases studied that the parasitic resonances are sufficiently distant from the operating frequency, such that no special measures are needed to suppress unwanted, close-by resonances.

Table 3: Coupling factors for modes closest to the TE011 operating mode (2.635 GHz).

f (MHz)	2483.173	2534.975	2578.719	2635.161		2804.22	2804.297	2867.93
Q (100 mm)	1.02E+07	1.31E+06	4.18E+03	1.49E+10		2.06E+09	2.85E+09	1.06E+06
f (MHz)	2483.14	2532.133		2.635.123	2662.625	2804.17	2804.228	2855.151
Q (90 mm)	3.42E+06	2.49E+06		1.50E+09	3.90E+03	3.41E+08	3.62E+08	8.94E+05

3.5) Field Enhancement

For an optimized cavity shape the field enhancement factor can be raised up to ~ 3.5 . Also, the TESLA single cell cavity can be stretched along its axis to increase the field enhancement factor. To adapt to a different shape cavity or to

accommodate possible modifications of the TESLA host cavity the host cavity cryostat was designed to be able to change its height by up to 2.5 cm.

3.6) Thermal Model

A numerical model was developed to simulate thermal issues in the sample and host cavity. It is obvious that the goal to produce magnetic surface RF fields beyond the currently achieved also leads to higher RF dissipation in the exposed surfaces. In particular it has to be pointed out that the measurement system proposed here operates at $f=2.635$ GHz, twice the frequency of the TESLA accelerating mode. With the major known surface resistance contribution, the so-called BCS resistance being proportional to f^2 the heat load is thus increased at least 4-fold at the same surface magnetic fields. Furthermore, it is the objective to achieve surface magnetic fields of up to $\mu_0 H=500$ mT on the sample, thus increasing the surface fields by ~ 2.5 beyond the best achieved so far in TESLA single cell cavities. The RF dissipation in the surface is proportional to H^2 , such that the heat load is boosted by another factor of 7.7. The following presents the results of calculations of the temperature rise in the sample as a result of RF dissipation. The formalism used is described in further detail in appendix A.

To calculate the surface temperature during short RF pulses a pseudo-transient model was developed. This model derives the temperature rise as a result of RF heating from the solution of a linearized heat balance equation. The RF dissipation is calculated from the BCS surface resistance R_s (to which a small, fixed residual resistance is added) and the peak field H_{peak} ($p_{RF}=R_s H_{peak}^2$). The temperature rise on the RF exposed surface during the short interval dt is calculated from the amount of heat $p_{RF}dt$ deposited during that interval (it is assumed that the pulse rise time is infinitely short). This infinitesimal heat increment is partly conducted out of the Nb wall through the Nb conductance and partly absorbed by the Nb enthalpy. The model takes into account the changing temperature in the calculation of the relevant material properties. The calculations assumed a simplified sample-holder design in which the helium and the RF exposed sample surface are separated by a 11 mm Nb bulk, thus neglecting the instrumentation spring (made of stainless) between the sample and the sample-holder, the cooling spring (made of Cu) between the sample-holder and the cold finger and the cold-finger wall (made of Cu). The thickness of all the elements just listed, however, adds up to that used in the model. Since in the pseudo-transient model the heat balance is applied to the entire Nb bulk (while in reality the heat is deposited only in a thin layer), it is only valid when the diffusion time is much shorter than the pulse time. At 2 K, however, the diffusion time in Nb as calculated from k and cp (see appendix A) is ~ 1 msec, close to the pulse-times of interest. This means that the model might actually under-estimate the local temperature rise. Also note that the model does not include the Kapitza thermal interface impedance between the Nb sheet and the He. It also does not include the possibility of film-boiling at fluxes exceeding the critical heat flux in helium II.

Fig. 12 shows the calculated surface temperature and surface resistance as a function of time during the rectangular RF pulse with different pulse amplitudes. There is clear evidence of thermal runaway after some ms for pulse amplitudes beyond 200 mT. The figure also shows the total surface power deposited as a function of time in the sample (using the simplifying assumption that the field is at its peak value over the entire sample). Given the thermal run-away problem it is necessary to limit the pulse duration. Fig. 13 shows the maximum pulse duration for

Conceptual Design of a Small Sample High Field RF Test Station

a rectangular pulse of given amplitude to limit the surface temperature rise to 100 mK. The plot shows that the pulse duration needs to be limited to 1 ms at ~200 mT and ~0.1 ms at 500 mT peak field. Also shown is the average RF power delivered to the sample during this pulse.

3.7) Plots

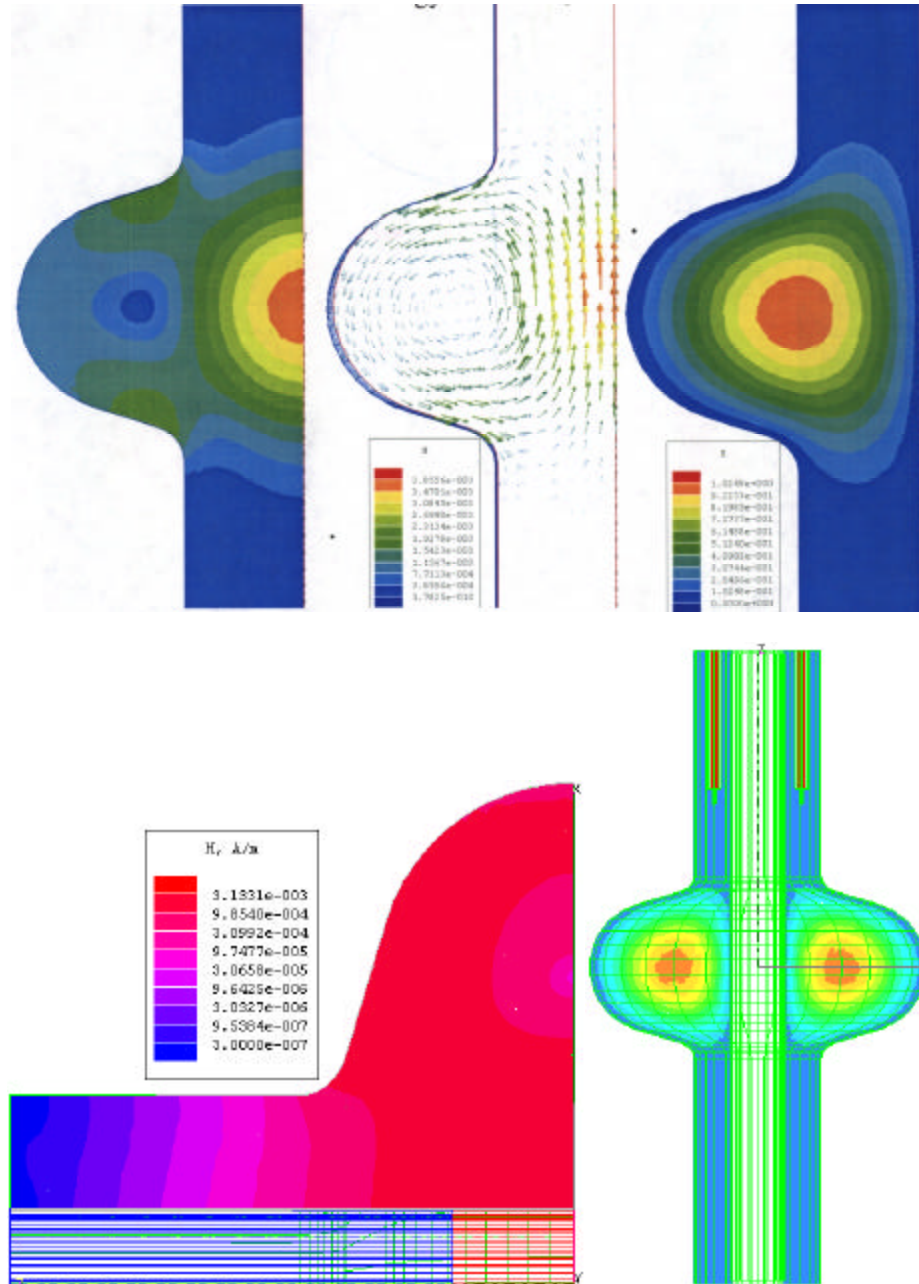


Figure 7: Field profiles for the TE₀₁₀ mode in single cell TESLA cavity. Magnetic fields – upper left and center, electric field – upper right plot. The magnetic field is highest at the position of the sample (upper center). The peak surface magnetic field on the host cavity is located between the iris and equator region (lower left). The complete cavity model is shown on the bottom right.

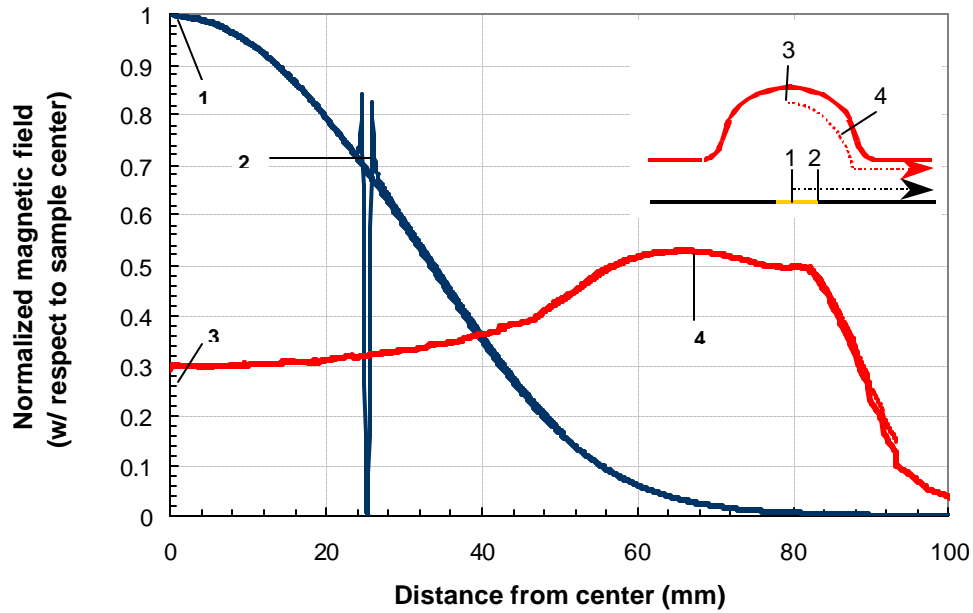


Figure 8: Result of HFSS computation of magnetic field along sample (including gap at edge of sample) and cavity. In this plot the magnetic field is normalized on the peak field at the sample. The sample dimensions assumed are 2x25 mm height, 31 mm outer \varnothing . The assumed edge shape is circular (0.5mm radius – see below for more on edge shape effects).

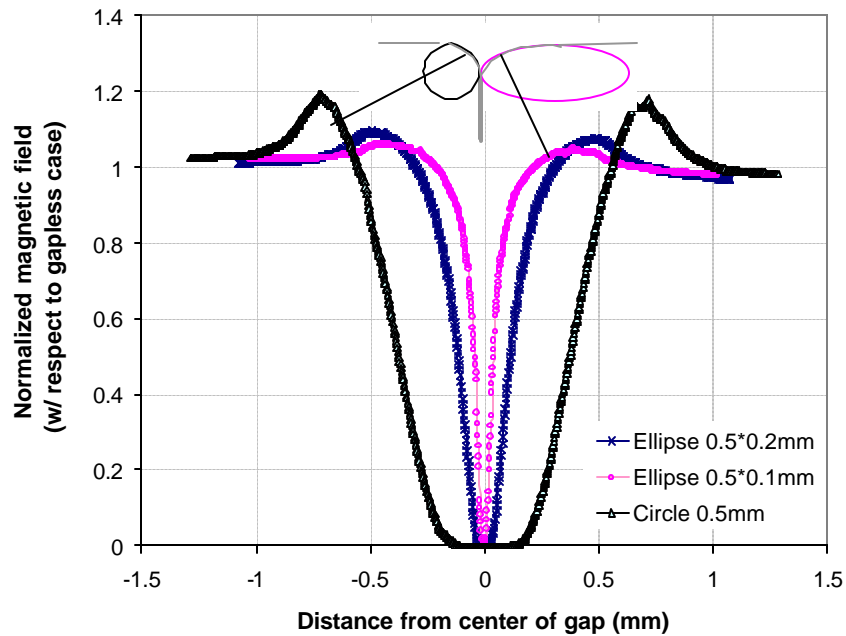


Figure 9: Results of HFSS computation of magnetic field enhancement at the sample edge, assuming different edge profiles (measures given are radius and half-axes, see insert). In this plot the magnetic field is normalized on the field in the “gap-less” case.

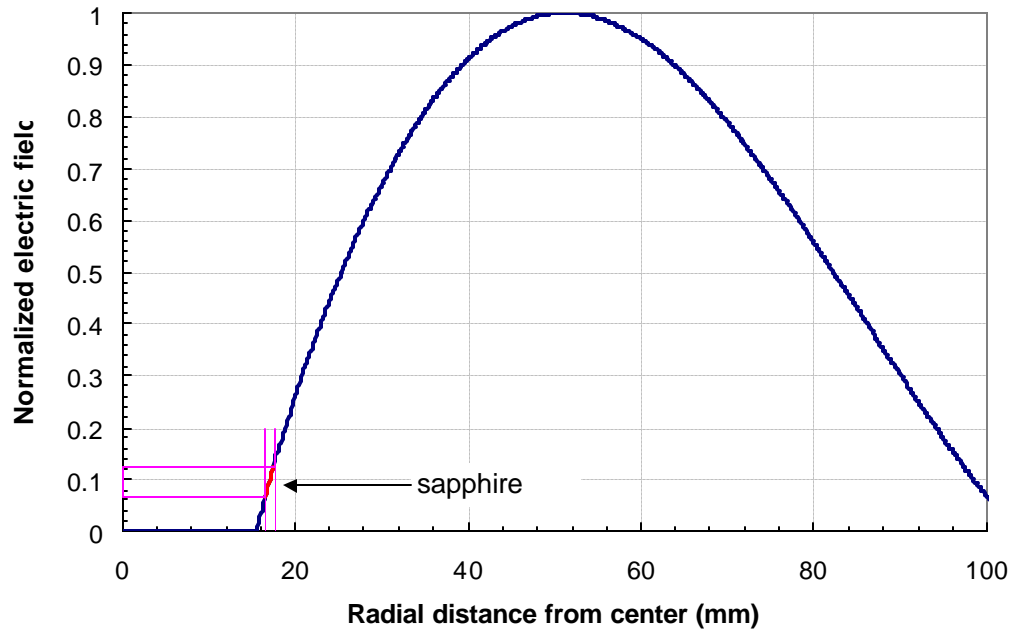


Figure 10: Normalized electric field along the radius from the center of the host cavity to the cavity equator. The electric field is zero on the inside of the sample (15.5 mm radius). The electric field at the location of the sapphire is typically 10% of the peak field.

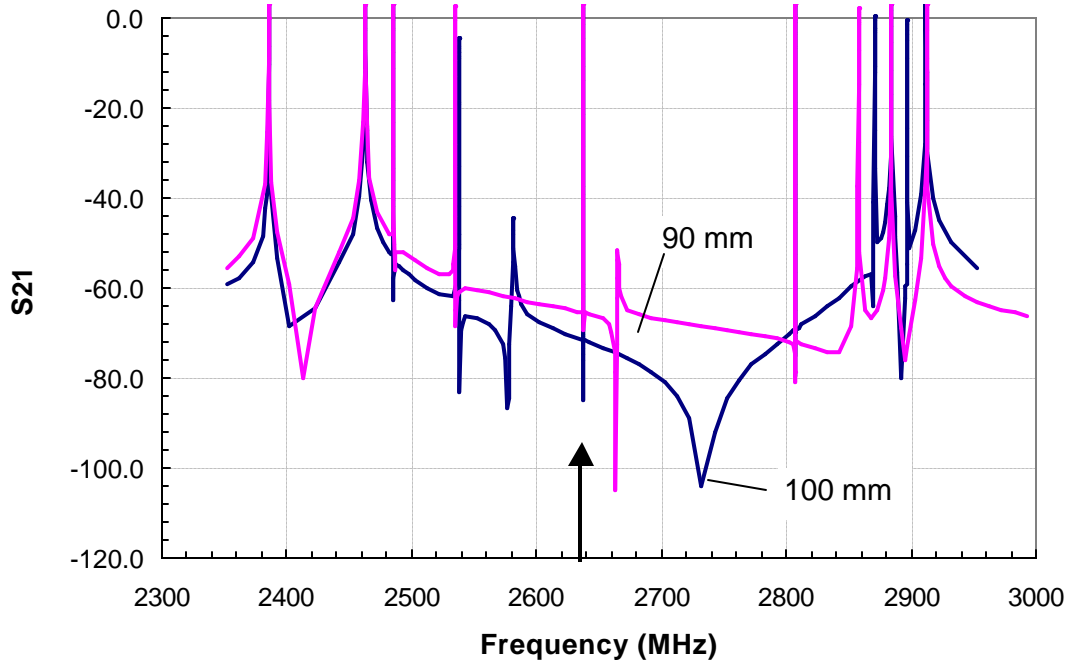


Figure 11: Coupling coefficient S_{21} between input and output antenna for two different coupler positions (both couplers are moved together) in arbitrary units: 100 mm / 90 mm distance from center to end of coupler loop (in the nominal position shown in Fig. 3 the distance is 111 mm). In the calculations the output coupler was always moved to the same depth as the input coupler.

Conceptual Design of a Small Sample High Field RF Test Station

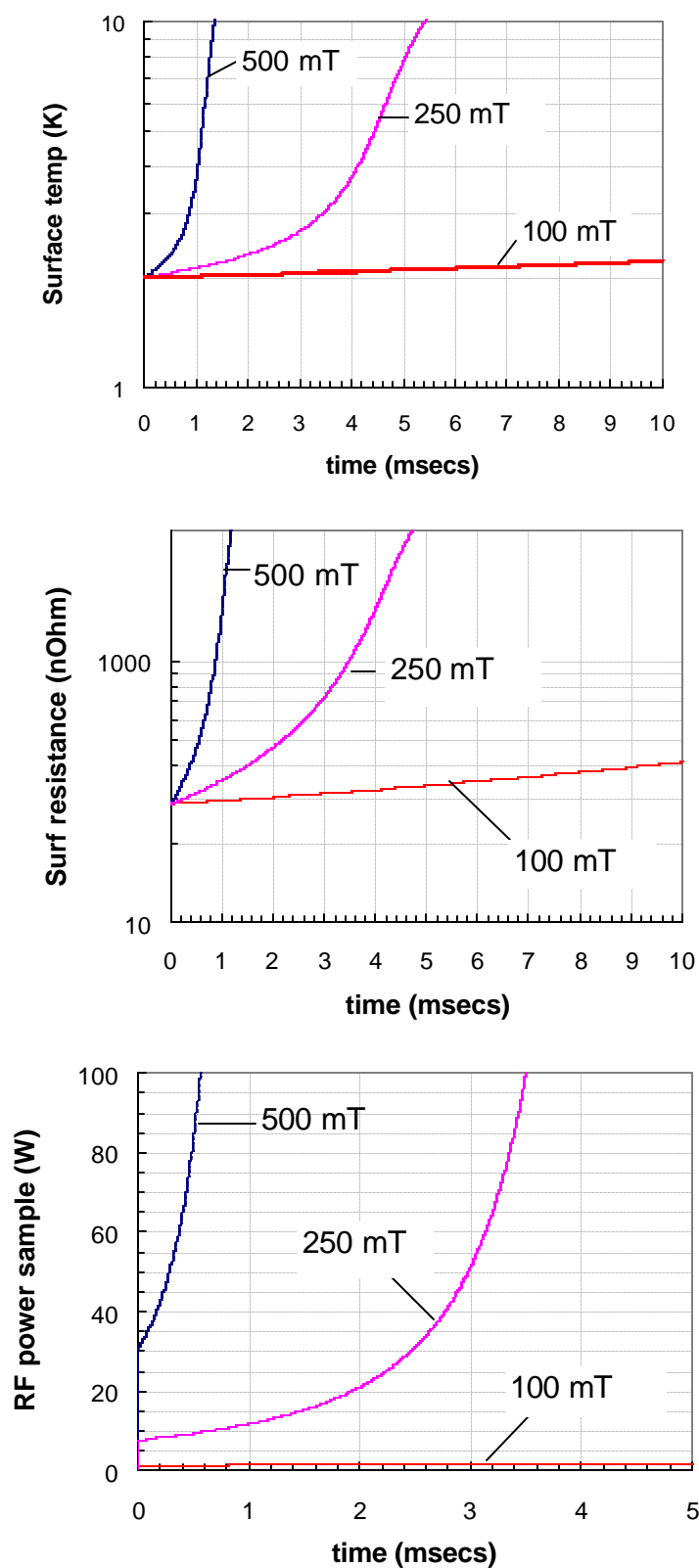


Figure 12: Surface temperature, surface resistance and total surface RF power in sample for different pulse fields. Note that the calculation assumes a rectangular pulse (zero fill-time), that the field is constant and at its peak value over the entire sample and that the heated surface is separated by 11 mm of Nb from the superfluid helium.

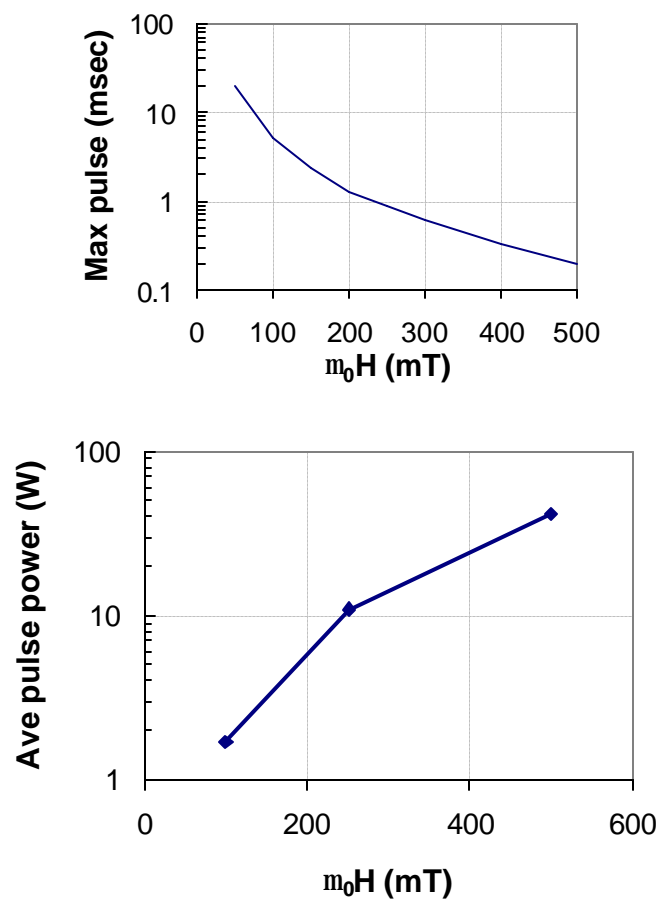


Figure 13: Upper: Calculated maximum RF pulse duration to limit surface temperature rise to 100 mK rise. Lower: Average pulse heating power in sample versus pulse amplitude. The calculation assumed the maximum pulse duration as shown in the plot above. Note that the calculation assumes -1- a rectangular pulse (zero fill-time) -2- that the field is constant and at its peak value over the entire sample and -3- that the heated surface is separated by a 11 mm thick of Nb sheet from the superfluid helium.

4) CRYO-SYSTEM

4.1) Basic Cryo-System Layout

The host cavity is cooled to $\sim 1.5\text{--}2\text{ K}$ with liquid helium using a combination of Joule-Thompson expansion and reduction of vapor pressure using strong pumps. This is a standard technology, used today in many superconducting RF systems. The sample cooling system uses a different approach. A cold finger cools the sample indirectly through conduction. The cold finger contains helium supplied from the host cavity bath. This approach allows cooling the host cavity and sample with the same cryo-system, while permitting independent regulation of the sample temperature with heaters (except that the sample cannot be cooled to a lower temperature than the host cavity bath temperature). The sample-holder slides over the cold finger, which is equipped with flexible copper blades to provide the thermal contact to the sample-holder. The feasibility of this particular cooling system design needs to be demonstrated beforehand (see step-by-step approach discussion in 13). Thermal calculations describing the cold finger cooling process in the cold finger are discussed below. Appendix C presents the cold finger thermal model calculations.

4.2) Dewar Design

To minimize the heat load to the host cavity cryo-system operating at $\sim 2\text{ K}$ and to reduce helium consumption during extended operation, a double-shield Dewar design is needed. The outer vessel needs to be approximately 2 m high and 1.5 m in diameter. Such Dewar designs are commercially available. They typically use a design such as shown in the schematic in Fig. 14. An outer $\sim 90\text{ K}$ shield cooled with LN and an inner $\sim 5\text{ K}$ shield cooled with LHe are surrounding the 2 K host cavity cryo-system. The LN shield

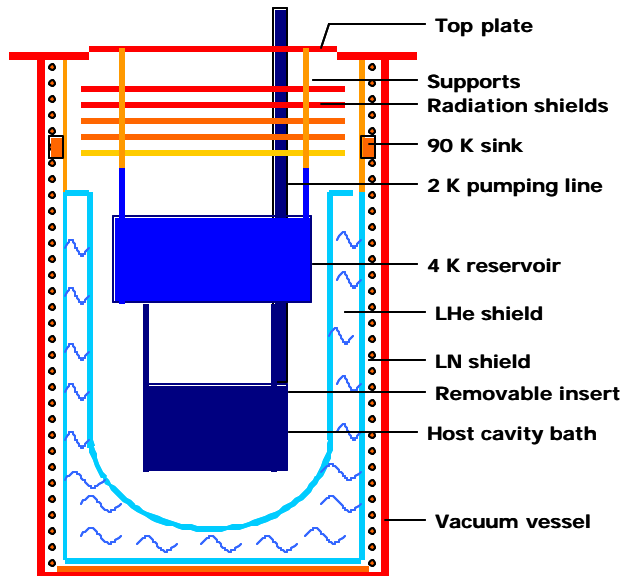


Figure 14: Schematic of Dewar with insert. MLI is not shown.

consists of a Cu coil mounted into the vacuum space between the helium vessel and the outer Dewar wall. The top of the liquid helium vessel is pre-cooled with the LN shield to 90 K to reduce the static heat leak. This pre-cooling stage typically consists of a massive Cu ring cooled actively by LN. Both shields hang from the top plate.

As shown in Fig. 14 the insert with the experimental apparatus is attached to the top-plate and includes thermal shields as well as 90 K and 5 K stages that shield the host cavity. These top shields are supplied independently from the Dewar shields and they serve more than

one purpose. The top 5 K shield, for instance, is the 5 K reservoir from which the host cavity cryo-system is provided with liquid helium.

The LN shield absorbs an estimated ~ 1 kW, mostly as a result of conduction from the room temperature top plate. In fact this heat load is almost entirely introduced through the top section (3 mm thick stainless) of the LHe shield, which is also cooled by the LN shield to reduce the static heat leak to the 5 K shield.

The 5 K shield in the Dewar, with a capacity of ~ 100 lit absorbs an estimated 15 W, which, given a latent heat of 20 J/g, corresponds to a boil-off rate of ~ 2 lit/hr. The largest fraction of heat is conduction from the 90 K stage at the top through the 3 mm stainless LHe cryostat wall. The 5 K shield is supplied by external 500 lit Dewars. As mentioned above the top part of the 5 K shield is the 5 K reservoir, which supplies the 2 K host cavity cryo-system. It is supplied independently from the Dewar shield. This reservoir holds also ~ 100 lit.

The goal of the Dewar design is to reduce the static heat leak into the host cavity cryo-system to < 300 mW and to reduce the total cryo-system liquid helium consumption to less than 0.05 lit/hr. To meet this ambitious goal it is necessary that all components connecting the low temperature components to the top plate, which is at room temperature, such as the support rods, cryo-tubes and instrumentation channels are pre-cooled with the 90 and 5 K shields. For example, the four support rods with which the entire insert is attached to the top plate are not continuous from top to bottom. Different rods support the host cavity cryostat from the 5 K reservoir than those attaching the reservoir to the Dewar top-plate. Also the reservoir suspension rods are in good thermal contact with the top LN shield. The same is done with the sample-channel, which passes through the 5 K reservoir for thermalization. It has to be noted also that the pressure drop across the JT valve will cause $\sim 15\%$ of the liquid supply to be evaporated immediately. The pre-cooling in the heat exchanger up stream of the JT valve mitigates this effect, but was taken into account in the lost fraction number quoted above.

Appendix B contains the formulas and material data used in the calculation of the cryo-system design heat loads quoted above.

4.3) Host Cavity Cooling System

The host cavity cryogenic system provides a stable 1.5-2 K bath to operate the host cavity. The host cavity bath is cooled with a combination of low temperature helium supplied from a JT expansion stage and through the reduction of the saturation vapor pressure with strong pumps. The helium supplied to the host cavity bath (through the JT expansion stage) is drawn from the LHe reservoir, which also, as discussed above, serves the purpose of thermal shield at the top. This reservoir is supplied from a liquefier or Dewars. LHe is pumped from the reservoir to the 2 K bath through a fully automatic JT valve. Before entering the JT valve, the transferred LHe is pre-cooled to ~ 3 K in a heat exchanger. The heat exchanger consists of a Cu tube coil (\varnothing 10 mm) mounted into the line through which the ~ 2 K GHe is pumped from the host cavity bath. The 4-5 K LHe enters the heat exchanger from the top where the gas is warmest and exits at the bottom where the pumped gas is at ~ 2 K. The temperature of the LHe at the exit of the heat exchanger is ~ 3 K. It is then pushed into the JT valve and after expansion its temperature drops to ~ 2 K. In addition the host cavity bath is cooled further via saturation vapor

reduction. A 50 mm diameter pumping line connects the 2 K bath to the pumping station.

The host cavity cryostat consists of stainless bottom and top plates (5 mm thick) welded to a stainless cylinder with slightly smaller diameter (50 cm OD, 3 mm thick). This diameter of the cryo-vessel was chosen such as to contain the host cavity and to provide additional space around the cavity for possible instrumentation (e.g. for temperature sensor array). The total host cavity volume is $\sim 0.6 \text{ m}^3$. The top and bottom plates have a $\sim 21 \text{ cm}$ diameter hole for the passage of the host cavity. In the lower portion of the vessel is a welded stainless bellows section that allows the cryostat vessel to expand vertically by up to 2.5 cm to adapt to changes of the host cavity size. The cryo-vessel height is stabilized with 4 titanium rods ($\sim 10 \text{ mm } \varnothing$) that rigidly connect the top and bottom plates, distributed symmetrically around the perimeter of the vessel. Their length is chosen to be exactly that of the host cavity (including the flanges) such that the cryo-vessel adapts to the exact size of the host cavity. Their length can be changed using shims in case the host cavity is stretched to increase the field enhancement factor. With Ti having a similar thermal contraction coefficient as Nb, the tie rods will force the vessel to shrink at the same rate as the cavity during cool-down.

Fig. 16 shows a sketch of the host cavity cryo-system. As shown in this figure the host cavity cryostat is filled completely with LHe, with the level extending into a smaller reservoir to the base of the 2 K pumping line. This is necessary in order to provide the overhead pressure required to prevent vapor-locking at the top of the cold finger. This issue is discussed in further detail below.

4.4) Sample Cooling System

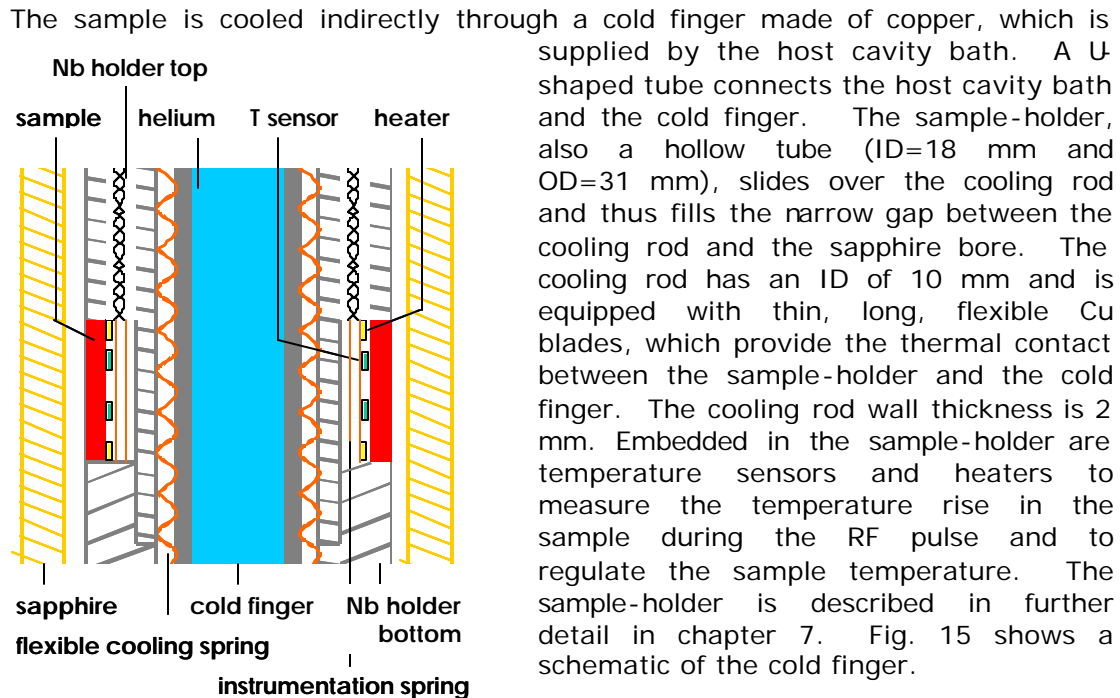


Figure 15: Detail of sample-holder cooling.

The cold finger design has the following advantages: It is mechanically

straightforward and simplifies greatly the design of the cryo-system. The sample can be inserted or removed without a need to provide or remove the liquid helium needed for cooling. The cold finger design also, through its poor thermal contact to the sample, provides the adiabatic condition during the short RF pulse required for the RF surface resistance measurement.

The cold finger cooling system has a fundamental issue: Even though the critical heat flux of superfluid helium and the diameter of the cold finger provide for sufficient heat transfer to evacuate the RF heating, any, even minute, temperature rise results in so called vapor locking because the bath is at the saturated vapor pressure condition. Even small quantities of evaporated liquid helium are trapped within the cold finger and lead to the expulsion of liquid, thus drastically reducing the heat transport and heat absorption capacity of the cold finger. To mitigate this effect the cold finger diameter needs to be as large as possible, the U-shaped connection tube between the cold finger and the host cavity bath needs to have a larger diameter such that it does not become the bottleneck for heat flux. Most importantly, however, the liquid level in the bath needs to be as much above the top of the cold finger as possible to prevent evaporation by overcoming the local decrease of saturation vapor pressure (e.g. due to a minute, local temperature rise) with hydrostatic pressure. Fig. 17 shows the calculated liquid overhead necessary to prevent gas formation in the cold finger for various values of steady state heat flux. The calculation shows that with an overhead of ~10 cm a steady state power of ~1 W can be absorbed by the cold finger. The details of the model are given in appendix C.

Since, as shown in Fig. 13, the peak pulse power (even after limiting the pulse length such as to prevent the sample surface temperature to rise) can be up to 70 W (with a reasonable overhead of 10-20 cm), vapor formation in the cold finger is to be expected during the pulse. Note, however, that the model used to compute the RF surface power shown in Fig. 13, does not take into account the thermal impedance separating the superfluid in the cold finger from the heated surface. This impedance will stretch the heat pulse in time and thus reduce its peak power. The finger helium volume is 23.56 cm^3 . At 1.9 K saturated vapor has a density of 0.609 mg/cc. As liquid is evaporated, vapor fills the finger, so in the end only the 0.0143 grams mass of vapor left in the finger has to absorb the latent heat of vaporization. The latent heat is 23.5 J/g, so the heat absorbed is 337 mJ. Therefore the heat deposited in a time of the order of 1 msec (100 mJ or less) is easily absorbed even in the case in which the helium in the cold finger has been vaporized.

4.5) Miscellaneous Systems

Additional hardware required for the small sample test-facility cryo-system consists of various pumping systems to provide the host cavity vacuum, the main dewar vacuum and the sample chamber vacuum. The usual diagnostics comprising various LHe meters (1-2 for each of the 3 cryo-containers - LHe shield, LHe reservoir, host cavity cryostat) and temperature sensors as well as pressure gauges are needed for the automatic control of the test facility cryo-operation.

4.6) Plots

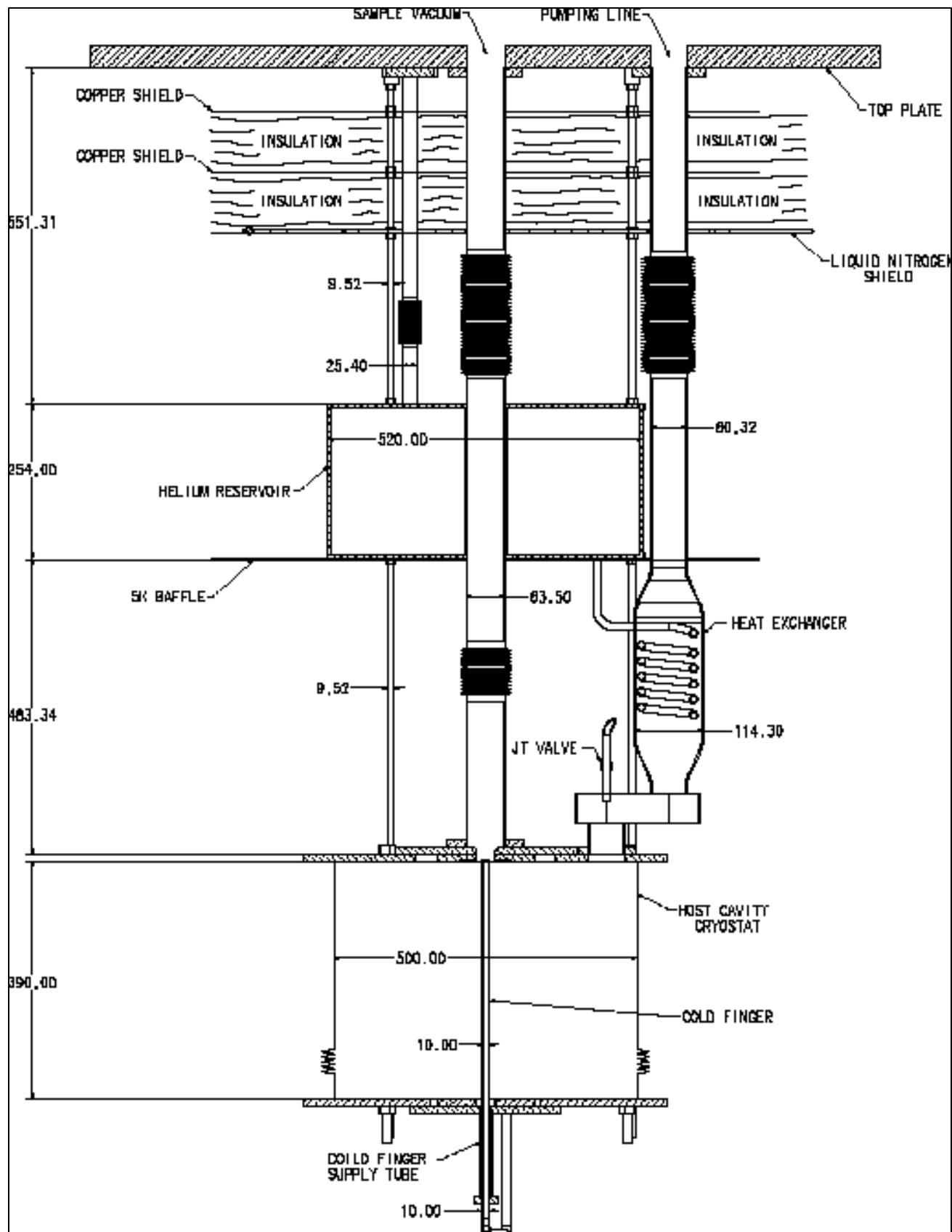


Figure 16: Host cavity cryo-system layout – all measures in mm.

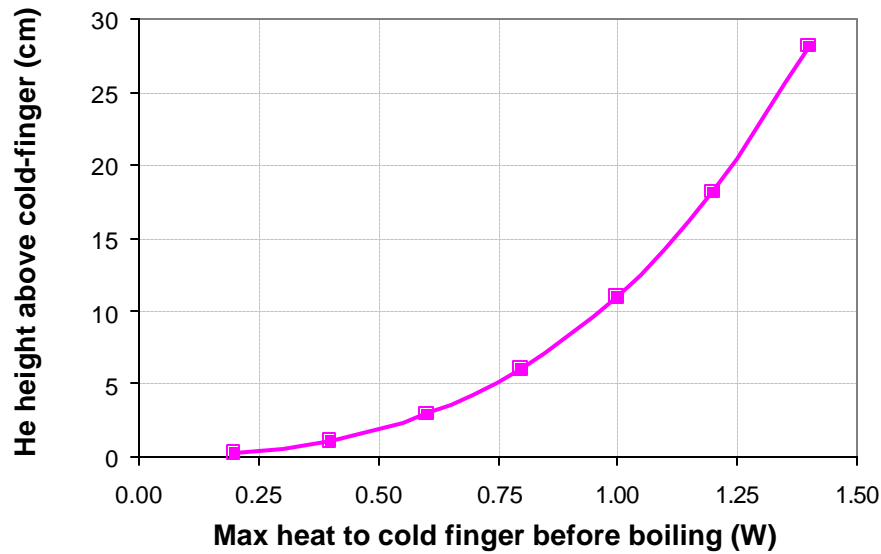


Figure 17: Plot of liquid overhead (i.e. difference of liquid level in host cavity bath to cold finger liquid level) needed to overcome gas-lock in cold finger as function of total heat input into cold finger.

5) SYSTEM ASSEMBLY PROCEDURE

The following describes the major steps of assembly of the small sample high field RF test system.

First the host cavity is prepared for assembly in the clean room. Tubing for the supply of the cavity with dry, filtered N_2 is attached to the cavity top and bottom. The host cavity cryostat is welded, assembled and cleaned. The Ti-rods are measured to have the appropriate length to adapt the cryostat height to the cavity size. After cleaning the cryostat is transferred to the clean-room. There the host cavity with the attached and sealed adaptor flanges and the sapphire bore in place is lowered into the cryostat through the opening in the top plate and placed on the bottom cryostat flange, already bolted to the cryostat bottom plate (Fig. 18). Then bolts are introduced into the cryostat bottom flange from below and screwed into the lower host cavity adaptor flange (the vacuum seal is provided by an Al gasket). At this stage the bottom cryostat flange is not equipped with the variable couplers, etc. They and the pumping line as well as the cold finger can be mounted once the cavity assembly is attached to the cryostat bottom flange. Fig. 18 (right) shows the step, which consists in attaching the variable couplers and the coupler drive system. The couplers are introduced into the holes of the cryostat bottom flange and the flanges are attached to the flange. Then the coupler guide flange and the attachment rods are screwed into the bottom cryostat flange. The pivot bars are attached. The vertical regulation rods, which connect the coupler pivot bars to the step-motor on the top of the cryostat will be attached later.

Meanwhile the assembly of the top portion of the insert can start. Fig. 19 shows the 2 K pumping line and the 5 K reservoir / sample vacuum channel assemblies. The pumping line, or chimney, consists of mostly welded stainless steel piping and

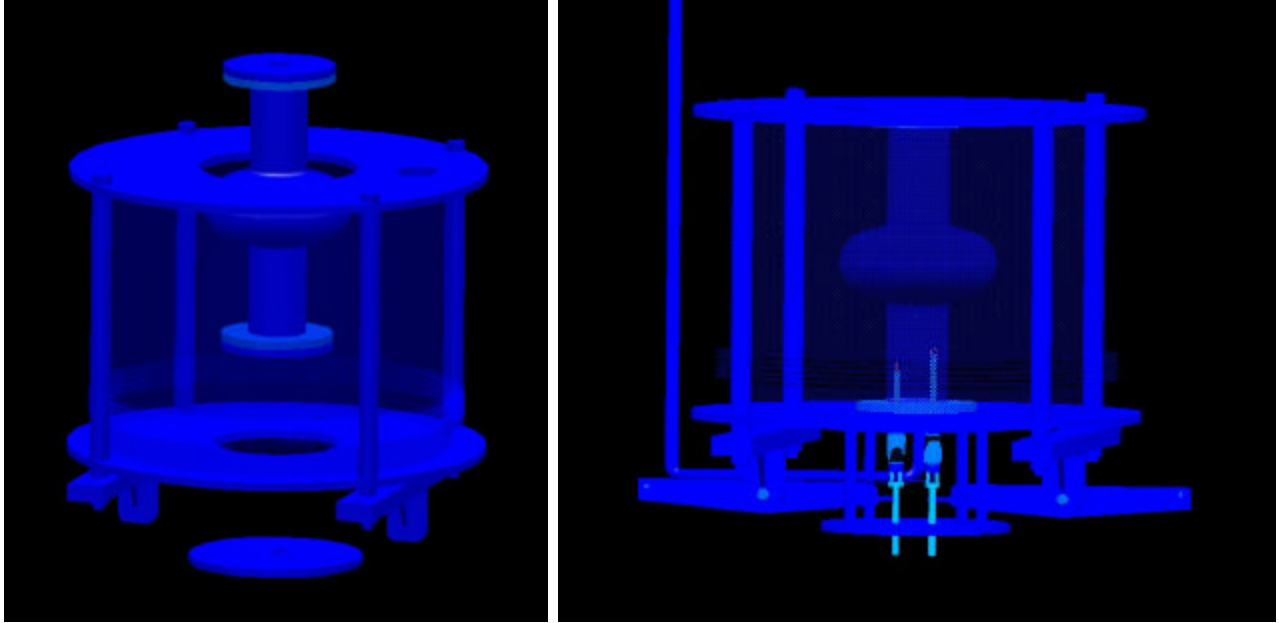


Figure 18: Left: Introducing the host cavity into the cryostat and attaching the bottom cryostat flange. Right: Attaching the couplers and coupler drive system.

connects the host cavity cryostat with the top plate. The bottom portion contains a helical heat exchanger, which allows the pre-cooling of the 5 K helium as it is pumped to the JT-valve. The heat-exchanger assembly is extended to the top by a simple pumping line including a bellows section to cope with thermal contraction and terminated with a flange with which it is affixed to the top plate. At the bottom the exchanger is welded to a small reservoir in which the superfluid helium level of the host cavity cryostat will be. The exit tube from the heat exchanger is routed to the JT valve and from the JT valve to the small reservoir. The 5 K reservoir consists of a simple cylindrical vessel with a tube through the middle through which the sample-holder can pass. Helium supply tubes are welded to it as well as brackets to which the rods on which the reservoir (and everything below it) will be suspended from the top plate. The top and bottom sections of the sample-holder vacuum chamber (including bellows) are welded to the reservoir such as to produce a continuous vacuum channel into which the sample-holder will be introduced later.

Fig. 20 shows the assembly of the entire insert. First the 5 K reservoir and sample vacuum channel as well as the pumping line are assembled into the array of thermal shields, most of them passive (some of them are cooled by LN with a cooling spiral). The shields are assembled along rods and covered with the needed number of MLI layers. This assembly is attached to the cryostat top plate. As a final step the host cavity cryostat is suspended from the 5 K reservoir on 2 crossbars that hang from 4 suspension rods, which are attached to the 5 K reservoir. The host cavity is contained within the magnetic shield. The sample vacuum channel and pumping line are affixed as well as the rods for the coupler drive system. Not shown in Fig. 20 are the wave-guides for the input coupler and the flexible coaxial line carrying the output coupler signal. Also the instrumentation and the respective wires are not included in the schematic. The insert is ready for installation in the Dewar. Not shown here are the elements mounted on the top plate such as the sample translation stage or the coupler drive system.

Conceptual Design of a Small Sample High Field RF Test Station

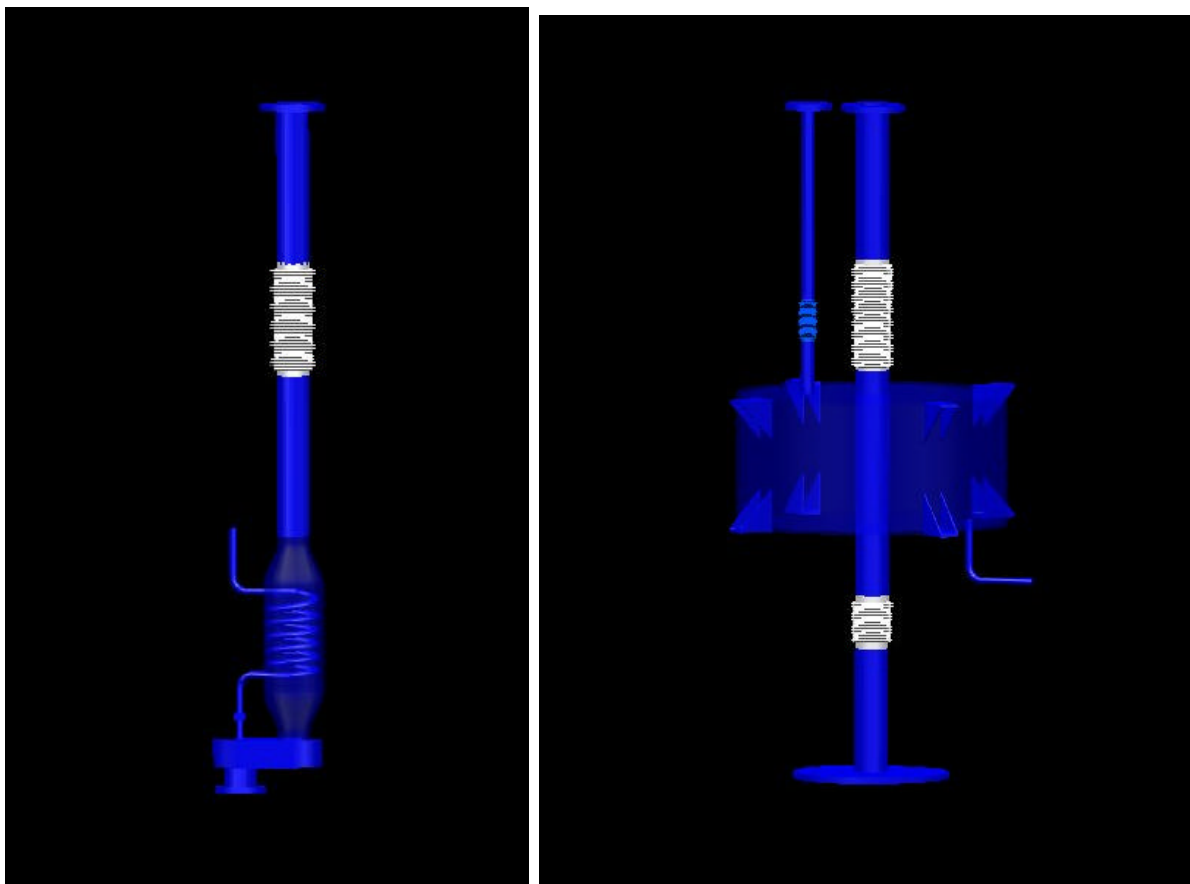


Figure 19: Left: Assembly of the 2 K pumping line (“chimney”); Right: Assembly of the 5 K reservoir and sample vacuum channel.

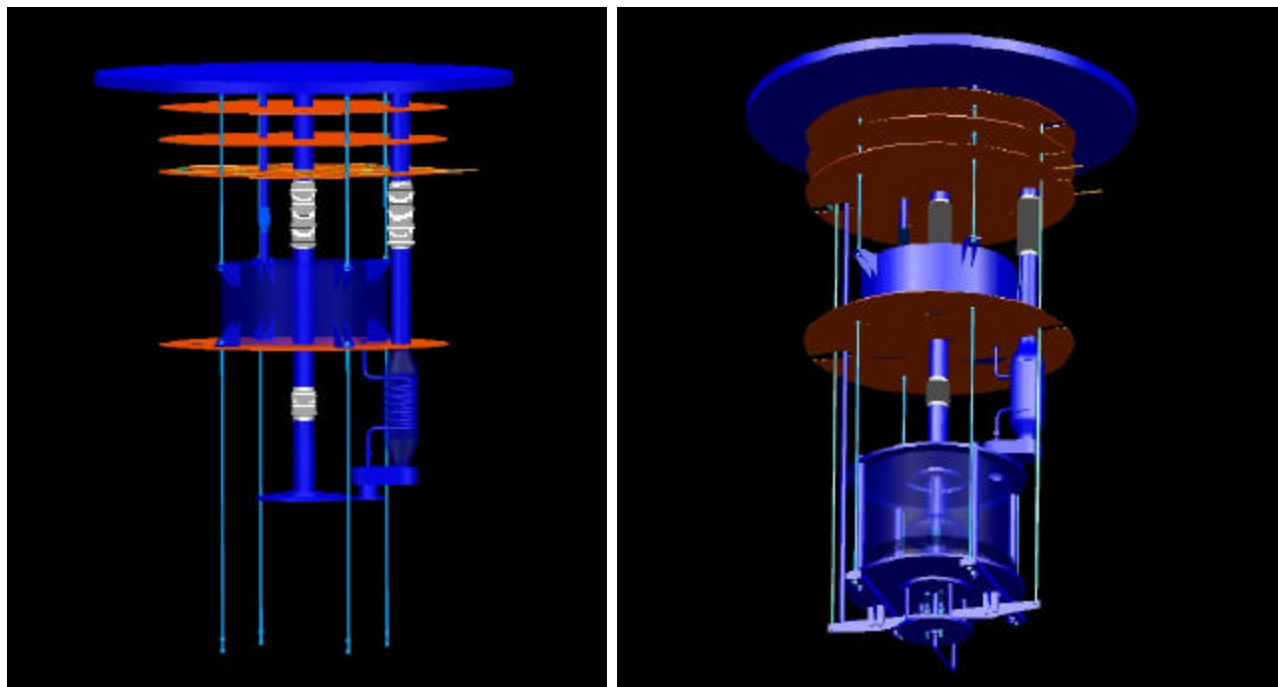


Figure 20: Insert assembly without (left) and with (right) host cavity cryostat.

6) RF-SYSTEM

6.1) RF Power Requirements

The RF system supplies power to the cavity. The power supplied to the RF cavity needs to be sufficient to overcome wall loss in the resonator, transmission losses and provide some overhead. This, however, can be achieved with low levels of RF power. As discussed in detail in chapter 3.6) the pulsed RF power is needed to prevent thermal run-away on the sample as a result of high RF power dissipation in very high fields. Pulse durations of 100 μsec to 1 msec demand fill-times as small as 10 μsec . A 100 μsec fill-time requires 40 kW. Traveling wave tube amplifiers cannot supply such power and a klystron type power supply is needed. The klystron represents the most expensive subsystem of the small sample test station. Some ideas are being presented in section 13, which, if proven feasible, could allow operation with longer pulses and thus eliminate the need for a klystron. The baseline design of the small sample test facility discussed here, however, is based on the use of a ~ 50 kW klystron.

6.2) RF System Design Outline

Fig. 21 illustrates the major components of the RF circuit needed to drive the host cavity and to perform the power and Q measurements. Not shown are diagnostic lines and secondary auxiliary equipment such as DC blockers, interlock circuitry, matching blocks and circulators. The pulsed RF signal, produced by the function generator is amplified by a TWTA and the klystron and sent through a low-loss wave-guide to the coaxial input coupler. Upstream of the input coupler is a directional coupler that couples out attenuated signals proportional to the incident and reflected waves. These signals are sent to the calibrated power-meter for measurement. The measured incident and reflected powers are needed to derive the power dissipated in the cavity, allowing determination of the unity coupling condition and the measurement of the cavity Q_0 . Following rectification in a diode detector the RF envelope of the reflected signal is also sent to the scope. The signal picked-up by the output coupler is also sent to a power meter and a scope. Since the output coupler is typically 100 times weaker coupled than the input coupler, the signal needs to be amplified (40 dB, low power) before the diagnostics station. The sharpness of the resonance in superconducting cavities requires the use of a feedback loop to maintain the resonance condition in the drive circuit in the presence of microphonics and Lorentz-force detuning. The phase-locked loop consists of combining the RF generator and cavity pick-up signals in a phase sensitive detector to determine the relative phase, which can then be minimized using a combination of manual phase shifting (rough) and automatic phase regulation (fine) in the RF source (FM). It is assumed that most of the phase shift occurs within the cavity.

6.3) RF Measurement System

The measurement procedure consists in raising the RF pulse height until the sample quenches. The combined Q_0 of the host-cavity and sample is the main parameter provided by the measurement. The unloaded quality factor of the cavity,

Q_0 can be derived from the measured loaded Q_L , which includes the external Q of the input couplers (as well as that of the output coupler, which is negligible). Q_L is commonly derived from the decay time constant of the exponentially decaying pick-up signal following a short RF pulse, which can then be multiplied by ω to produce Q_L . The unloaded quality factor can easily be obtained from the loaded quality factor in the case of unity coupling ($Q_0=2Q_L$). Since in practice the coupling coefficient is not perfectly 1, it needs to be measured. Typically the coupling factor is derived from the measured ratio of reflected and incident power.

At high field levels, however, the loaded quality factor and therefore also the time constant are field dependent and thus change as power is drained from the cavity. This complicates the derivation of the decay time constant. Therefore it is often preferable to measure Q_0 from the pick-up signal at the pulse flat top directly. The pick-up signal is proportional to the stored energy in the cavity. It can be combined with the measured dissipated power, i.e. the difference of incident power and reflected power, to give the cavity Q_0 . For this measurement the pick-up signal needs to be calibrated. A possible pick-up calibration technique involves measurements of the kind described above, but in cw conditions at low power.

These methods, however, describe the measurement of the combined Q_0 of the host cavity and the sample. Section 8 discusses in further detail what technique is used to extract the sample surface resistance from the combined Q_0 .

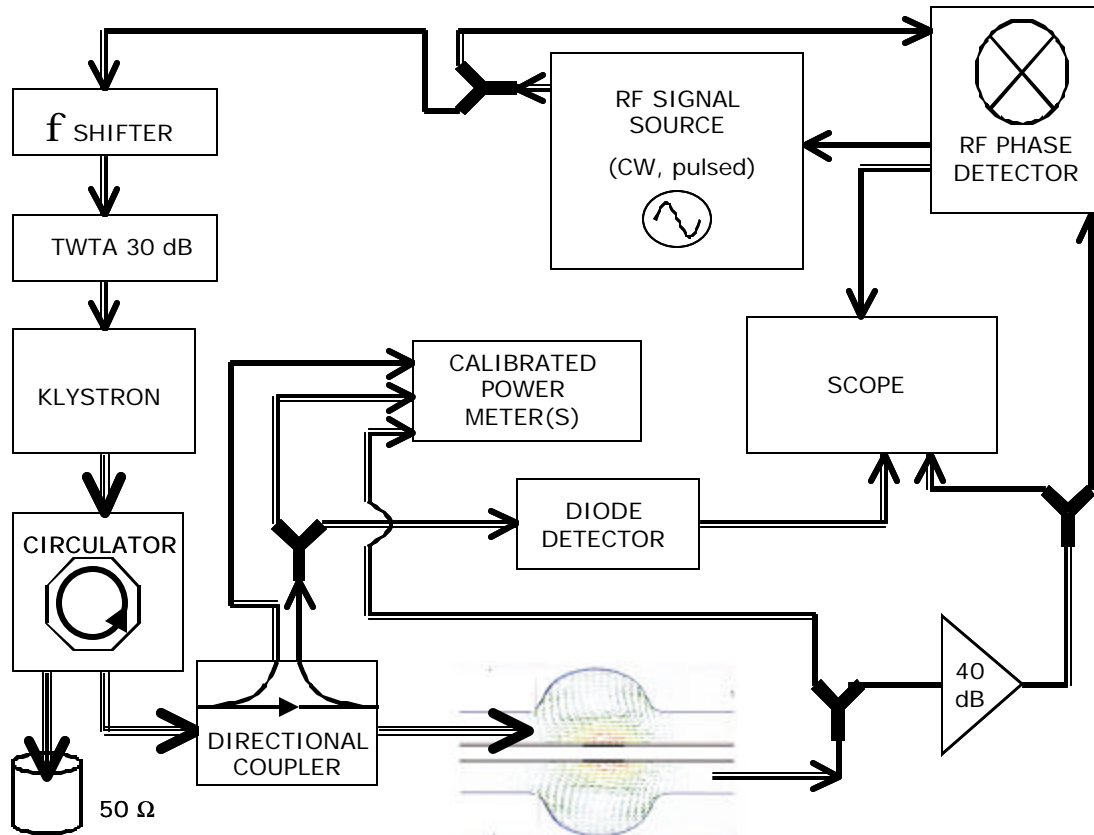


Figure 21: Outline of the experimental set-up – RF system.

7) SAMPLE-HOLDER and SAMPLE-TRANSFER STAGE

7.1) Sample-Holder Design

The sample is introduced into the high magnetic field region in the host cavity with a sample-holder, which is lowered into the test-station with a x-y-z translation stage (shown in Fig. 23). Fig. 22 shows a sketch of the sample-holder. The upper portion has a larger diameter and is made of stainless steel. The lower portion is made of Nb and contains the sample. In the fully withdrawn condition, which allows exchange of the sample in the load lock chamber above the cryo-stat top-plate, the translation stage bellows are fully extended upwards. When lowered into the station

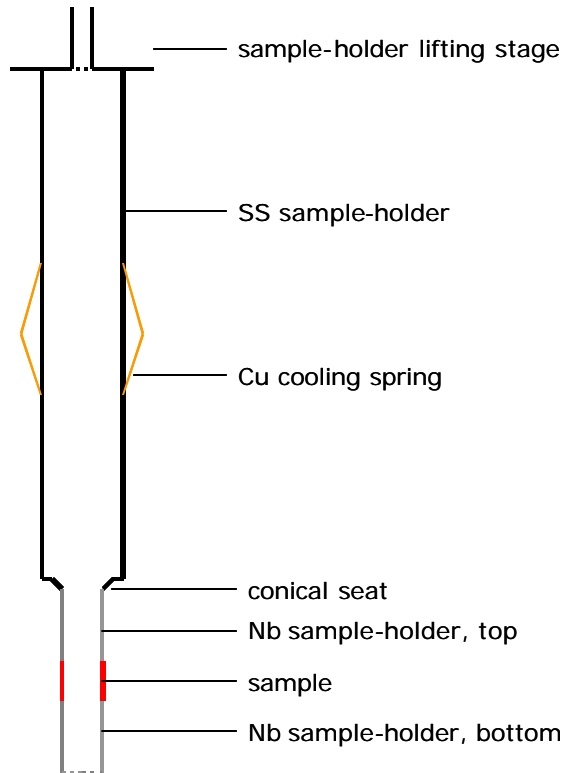


Figure 22: Schematic drawing of sample-holder.

the sample-holder is first introduced into the upper sample vacuum channel, which extends from the gate valve (now open) to the top of the host cavity cryostat as well as into the host cavity. The sample vacuum channel has an ID of ~6.5 cm and consists of 4 sections. The first part from the top connects the gate valve to the 5 K reservoir. The second part crosses the channel through the middle of the 5 K reservoir, where the sample-holder is pre-cooled to ~5 K (To that end the sample-holder is equipped with flexible Cu blades, which establish the thermal contact between the sample-holder and the vacuum channel wall.) The third part connects the reservoir to the host cavity cryostat top flange. The fourth part runs within the sapphire bore in the host cavity. Interspersed between sections are bellows to cope with differential thermal contraction issues and to reduce heat conduction to the 5 K and 2 K stages. The

bellows are welded on the reservoir side and bolted with vacuum tight flanges to the top plate and host cavity cryostat top plate at their respective ends. Within the host cavity the sapphire bore serves as the sample vacuum chamber. Note that the sapphire bore is only loosely assembled into the host cavity, such that in fact there is a weak coupling between the sample and host cavity vacuum systems (which is therefore regarded as one system).

The upper sample-holder stainless steel section and the lower Nb part with the smaller diameter are joined by a welded bell-reducer. The fact that the lower portion of the sample-holder has less OD than the upper part ensures that the sample can be lowered into the host cavity without being damaged. The bell-reducer is made of Nb and, once the sample-holder in place, fits into a matching cone machined into the cryostat top flange. This contact closes a possible RF field leak. Below the bell-

reducer starts the part of the sample holder, which will be exposed to the cavity fields. Ideally it should also be removable (e.g. by unscrewing) so that the cavity can be tested without any insert. In this case a Nb lid would be screwed into the bell reducer, which would essentially close the cavity to contain the RF fields.

The lower part of the sample-holder in fact consists of 2 parts, screwed into each other with the sample wedged in between. The lower part can be disassembled by unscrewing it from the top part to allow for removal of the sample. Once the lower part is removed, the sample can slide down over the threaded portion of the upper part. It is important that the sample-holder OD within the cavity is constant. Also, the section of the sample-holder that is inside the cavity is exposed to RF fields and therefore has to be made from high purity Nb with a state of the art surface finish to prevent Q degradation in the host cavity. The sample is 5 cm long, so that the edges between the sample and the sample-holder are outside the high magnetic field region. Within the host cavity the sample-holder tube OD is 31 mm, fitting into the sapphire bore which has an OD of 35 mm. Assuming a sapphire wall thickness of 1 mm, there remains a 1 mm gap between the sample-holder and the sapphire bore. The wall thickness of the sample-holder within the host cavity is 6.5 mm. On its inside is a 2 mm gap to the cooling tube. This gap is bridged by the cooling springs.

7.2) Sample and Sample Instrumentation

If made from a sheet, the sample could be manufactured by rolling and e-beam welding. Since this procedure would not produce a perfectly cylindrical sample with the specified diameter, additional machining of the sample is certainly needed. The ID of the sample also needs to be increased (in general) to ~29 mm to provide sufficient space between the sample-holder and the sample for the heaters and temperature sensors. A ~2 mm annular gap is currently assumed. See Fig. 6 for details of the sample dimensions. Fig. 15 shows a sketch of the sample and sample-holder in the high field region.

A spring-based system is being envisaged to press the heaters and temperature sensors against the sample. A ~0.5 mm thick steel sheet, as wide as the sample and long enough to make one turn around the sample-holder is welded to the sample-holder section behind the sample. This sheet plays the role of a stiff spring that presses heaters and temperature sensors against the sample. The four Cernox temperature sensors (~1 mm², 1 mm thick) are mounted on the sheet along a vertical line (since the system has azimuthal symmetry it is not necessary to measure the temperature at different azimuths). At the top and bottom rim of the spring are two ~1W strip heaters. Using polyimide tape the strip heaters are brought up to the same OD as the temperature sensors. The wires supplying the heaters and reading out the temperature wires are collected and brought up through two holes within the wall of the upper part of the Nb sample-holder tube. Once out of the cavity the wires can be routed through the core of the stainless tube, which constitutes the top part of the sample-holder.

7.3) Sample Exchange Procedure

The facility does not have to operate in a clean-room environment, if the sample channel and the host cavity are under vacuum at all times. As outlined below

precautions have to be taken to prevent contamination of the sample and sapphire bore during sample exchange. A gate valve seals the sample exchange chamber from the sample vacuum channel leading down into the host cavity. While open to air for the sample exchange, the preparation chamber should be supplied with a large flow of dry, filtered nitrogen to prevent settling of airborne contaminants. The sample should be passed into the preparation chamber through a small hatch and mounted using gloves. After sample exchange the preparation chamber is evacuated and out-gassed with powerful (external) heaters. Once the RGA indicates pressure levels below 10^{-9} mbar, the gate valve is opened and the sample is lowered into the sample vacuum channel with a vertical sample transfer system (see Fig. 23). The sample-holder is lowered slowly into the sample vacuum channel to allow time for

cooling in the 5 K pre-cooler stage. Once the sample has reached 5 K it can be lowered

After the completion of a measurement run, the sample is extracted from the host cavity by pulling it up with the vertical sample transfer system. The gate valve separating the load-lock from the sample vacuum channel is in the open position during that stage to allow passage of the sample instrumentation wires. Once the sample-holder is entirely retracted, the gate valve is closed and thus the load-lock vacuum system becomes separated from the sample vacuum system. The load-lock chamber is then flooded with flowing, dry, filtered nitrogen and once the pressure is above ambient the access-window can be opened for sample exchange.

Fig. 23 shows an example of a commercial vertical sample transfer system, or Omniax™, that moves the sample from the sample exchange chamber (or load lock), into the host cavity. This system allows for fine-adjustment in x-y (10 mm tuning range) and has a stroke of 150 cm in z. It is mounted on top of the load-lock chamber and consists of a mechanical frame, along which the sample is pulled up. To maintain the sample vacuum, the sample is enclosed in a flexible channel made of

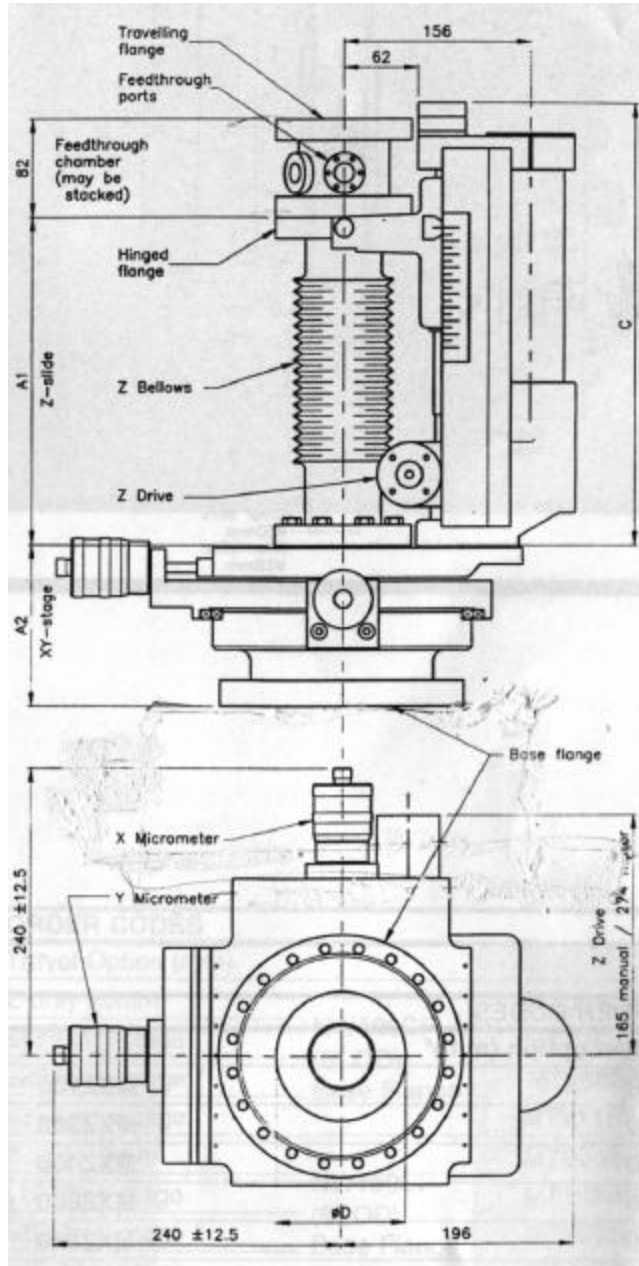


Figure 23: Omniax™ sample transfer stage.

bellows. In the fully retracted position the bellows are fully stretched and the bottom of the sample-holder is positioned at sufficient distance from the gate valve to allow disassembly of the sample-holder. The removal of the sample consists of unscrewing and removing the 17 cm long bottom part of the sample-holder. Great care has to be taken to ensure that the Omniax™ is driving the sample into the right position, requiring good alignment of the load-lock chamber top plate, the sample vacuum channel, the host cavity top plate, the cold finger and the sapphire bore. Alignment measurements need to be performed on the system after a dry assembly. An additional requirement is that the sample translation stage is capable of applying pressure to the sample to ensure that the additional cooling of the sample-holder is provided through the thermal contact with the top and bottom flanges of the sapphire bore. Also to be taken into account is the vertical extension of the Omniax™ frame when designing the test-station environment (it affects the pit-depth and the design of the radiation shield on top). The translation stage also needs a UHV type feed-through for the sample instrumentation wires.

The load-lock chamber is ~50 cm high and ~30 cm in diameter. It is bolted to the gate valve, which in turn is affixed to the cryostat top plate. The sample transfer system is affixed to its top. For passage of the sample the load-lock chamber has round holes roughly the size of the diameter of the sample-holder in the center of its top and bottom plates. It also has a wide pumping port as well as a port for the supply of nitrogen gas. Both ports have to be equipped with UHV compatible valves. Most importantly, however, the load-lock chamber has access windows that allow a person to reach into the load-lock chamber and replace the sample.

8) MEASUREMENT TECHNIQUE

The goal of the here described measurement system is to measure the surface resistance and the critical magnetic RF field of small superconducting samples in high power RF conditions (at ~ GHz frequencies). Two parallel measurement methods are proposed to measure the surface resistance, the Q-perturbation and the thermometric methods. The host resonator for sample measurements should preferably have a very high Q factor so that the sample contributes a large portion of the microwave losses. The goal is to achieve $Q_0 \sim 10^{10}$ in the host cavity with the central Nb rod. Pulsed measurements benefit both measurement techniques. Both methods are discussed in the following.

8.1) Q Perturbation Method

The surface resistance of the sample can be derived from the Q_0 of the sample plus cavity system. Very large Q factors can be measured using the relaxation method³. The output coupler (pick-up) signal generated during and after an input pulse signal with frequency ω_0 is measured using oscilloscopes. At the end of the input pulse, the pick-up signal decays exponentially with a characteristic decay time $t=Q/\omega_0$, which is ~4 secs in the case discussed here. The measured Q factor is the

³ A. Proch, "Microwave Impedance", p. 1415 in "Handbook of Superconducting Materials", Institute of Physics, O.A. Cardwell, D.S. Ginley editors

loaded quality factor Q_L , which includes the effect of the couplers and which decreases with increasing coupling strength. In the limit of weak coupling $Q_L \sim Q_0$. In the case of so-called unity coupling (no power is reflected from the cavity) $Q_L \sim 2Q_0$. In case weak or unity coupling cannot be achieved, there are straightforward corrections to determine Q_0 from Q_L using measurements of the incident and reflected RF power (equation 1). Issues with this technique are the field (time) dependence of the decay time constant from which the loaded Q is derived as well as perturbative high field phenomena such as field emission.

$$Q_0 = Q_L(1 + b); \quad b = \frac{\left(1 + \sqrt{\frac{P_{reflect}}{P_{in}}}\right)}{\left(1 - \sqrt{\frac{P_{reflect}}{P_{in}}}\right)} \quad (1)$$

The method discussed above yields the Q_0 produced by the sum of the sample and the host cavity. To discriminate between the two contributions a reference measurement is performed with a sample with the same surface resistance as the host cavity. In this case the surface resistance contribution of the sample can be derived from the calculated "fill-factor" of the sample. The fill-factor is the fraction of RF power dissipation on the surface of the sample with respect to the total dissipation, ~22% in our case. It is calculated from the integral of the magnetic field over the sample as well as the cavity surface. The change of Q produced by a particular sample with respect to a reference sample is derived from changes in the field decay characteristic. More precisely, the Q perturbation method consists in measuring the difference of the Q_0 from the decay curve time constant following a pulsed excitation of the cavity with a reference sample and with the sample, attributing any change to the difference of surface resistance of the sample with respect to the reference sample. Equation (2) shows how the sample surface resistance can be calculated from the Q_0 measured with the reference sample, Q_{ref} , and that measured with the sample of interest, Q_s . Equation (2) assumes that the surface resistance of the reference sample is the same as that of the host cavity. The surface resistance of the host cavity, R_{cav} , is also needed to derive the surface resistance of the sample in absolute, as well as the filling factor a (which is usually calculated).

$$R_s = R_{cav} \left(\frac{Q_{ref}}{Q_s} + \frac{Q_{ref} - Q_s}{aQ_s} \right) (\Omega) \quad (2)$$

There is, however, an alternate method, which consists in determining the surface resistance of a sample directly from the measured cavity field (or voltage in pick-up V) and dissipated power (P_{diss}). This procedure also requires the exact knowledge of the surface resistance of the cavity with the reference sample and a well-calibrated pick-up. For a discussion of a possible pick-up calibration procedure see chapter 6.3.

8.2) Thermometric Method

In addition, an independent, second surface resistance measurement method using precision thermometers is proposed. The thermometric method derives the surface resistance of the sample during the RF pulse from the temperature rise of the sample. With a resolution of 1 mK, which is less ambitious than the best achieved, a resolution at the $n\Omega$ surface resistance level can be achieved. The calculated dissipation in the sample at 250 mT surface field and 100 $n\Omega$ surface resistance is ~ 0.6 W, large enough to produce several K temperature rise in the sample during a 10 msec pulse. Assuming a 31 mm OD, 50 mm height and 2 mm thick sample, a temperature rise of several 100mK/msec is expected. This thermal run-away issue, which is discussed in detail in chapter 3.6, is the reason why the RF power needs to be pulsed, with shorter pulse duration the higher the pulse field amplitude. For the thermometric method to work, however, it is necessary to insulate the sample thermally from any source of cooling. The Cernox temperature sensors have to be mounted on the sample holder, such as to be in good thermal contact with the sample and shielded from the RF fields. With fast pulsed measurements the time resolution of Cernox sensors (currently 1 msec at best) becomes the major limitation of the thermo-metric method.

8.3) Quench Field Measurement

Given that the surface temperature can be stabilized as a result of shortening the pulse length, the quench field can be easily determined as the surface peak field on the sample at which the temperature runs away (and the Q suddenly drops) despite the short pulse length. If working properly, both methods should therefore allow very accurate quench field measurements.

9) SAPPHIRE COLD BORE

The sapphire bore separates the host cavity vacuum from the sample vacuum and therefore allows sample exchange without removing the host cavity from the cryostat. Since the sapphire tube is therefore exposed to RF fields. The low loss tangent of sapphire (down to 10^{-10} at 10 GHz and liquid helium temperatures) is the reason why it was chosen for that purpose. Single crystal sapphire tubes with 99.9% purity and up to a length of 1m are now commercially available in the diameters needed for our application. For mechanical robustness we believe a 20 mm outer diameter sapphire tube with a 1 mm wall thickness represents a reasonable choice. Sapphire is usually polished in H_3PO_4 . Additional high-pressure water rinsing such as is the standard for the Nb components would be applied at Fermilab. The brazing to NbTi flanges at the ends requires a metal substrate layer, which is usually evaporated on the sapphire. Such a substrate layer is typically Kovar, a Fe-Ni-Co alloy with thermal expansion characteristics very close to that of glass and ceramics. Unfortunately Kovar is ferromagnetic and since it is within the magnetic shield of the test-station it is feared that it could contaminate the test volume with residual field. It is not clear yet whether a thin, 1 μm layer of Kovar is a concern. Other material properties of importance are discussed in the following. The thermal conductivity of single crystal sapphire (along the main crystal-axis) 40

W/m/K at room temperature and even higher at cryogenic temperatures. Sapphire is therefore an excellent conductor of heat and the temperature gradient from the ends to the middle of a 1 m sapphire tube with a 20 mm OD and 1 mm thick wall is thus negligible. The thermal shrinkage of single crystal sapphire along the cylinder axis is $\sim 5 \times 10^{-6}/\text{K}$ at room temperature and drops by 3 orders of magnitude toward low temperature. A rough estimate of the integrated thermal shrinkage between ambient and 10 K on the basis of published data⁴ is ~ 0.3 mm/m. The change in tube ID, which is ~ 20 mm, is therefore ~ 6 μm . Since most of the components of the host cavity assembly are made of Nb, it is the differential thermal contraction coefficient of Nb and Sapphire that is important. The integrated thermal shrinkage of Nb is 1.43 mm/m, thus ~ 5 times larger. For that reason, to avoid Kovar coating as well as because it simplifies the design considerably, the sapphire bore is only “loosely” assembled into the host cavity in the current design.

Fig. 3 shows how the sapphire bore is assembled into the host cavity of the small sample high power test station. The sapphire bore is mounted into grooves in the host cavity adaptor flanges. The groove in the top adaptor flange has extra depth to accommodate for the smaller thermal shrinkage of sapphire during cool-down.

The sapphire cold bore is exposed to high magnetic fields. Only single-crystal sapphire, with a loss tangent in the 10^{-8} - 10^{-10} range can sustain 200 mT RF fields with negligible heating. There is also a concern that the sapphire could be a strong field emitter causing multipacting. Calculations indicate that the electric surface fields in the sapphire with an OD of 35 mm should be below ~ 5 MV/m. Ceramic RF windows in high power couplers typically show signs of strong field emission at fields in excess of comparable field levels MV/m. Preliminary tests of the field emission behavior are necessary steps to a successful implementation of the sapphire bore idea.

10) MAGNETIC SHIELDING

To shield the host cavity and sample from magnetic fields exceeding $1 \mu\text{T}$, a 2-layered Cryoperm[®] shield (1 mm wall thickness) is assembled around the host cavity cryostat. Fig. 24 shows an example of such shield as built by Amuneal Inc.. The shield consists of a 0.8 m high, 0.8 m diameter barrel, which slides over the host cavity cryostat from below. In fact the host cavity is lowered into the magnetic shield. The sidewalls are assembled into grooves machined into the bottom plates. There are ~ 5 cm of distance between the shield walls. Calculations indicate that such a shield can yield 45-fold attenuation of the external field, which, in the case the external field is approximately the earth's field, is sufficient to attain the stated goal. The shield is mounted on 2 crossbars, which are suspended with 4 rods from the 5 K reservoir. The host cavity cryostat is placed into the magnetic shield. Therefore the shield is at ~ 2 K. Nitronic 40 steel is suggested as material for the host cavity cryostat because of its low magnetic permeability. The top-plate of the shield is complicated by penetrations for the sample vacuum chamber, instrumentation channels and most importantly the 2 K pumping chimney. Tabulations are required to shield those penetrations. The rule of thumb is to make the tabulations 3 times the diameter of the penetration, raising the height of the

⁴ M. Tobar, J. Krupka, E. Ivanov, R. Woode, “Dielectric frequency-temperature-compensated microwave whispering-gallery-mode resonators”, J. Appl. Phys. 38, pp 2770, 1997



Figure 24: Magnetic shield.

shield. The tabulations are added on both sides of the plate. The bottom-plate of the shield includes tabulations for the cavity pumping port and the variable couplers. All corners of the shield are strengthened with special Cryoperm[®] parts. It is important that the Cryoperm[®] plates, "corners" and tubes are re-annealed following machining and a dry assembly. Also test-measurements on the fully assembled shield with NMR gages are needed to confirm that the final assembly of the shield is working to specs.

11) VARIABLE COUPLERS

The TE₀₁₀ mode is best excited in the cavity with a co-axial input coupler with a shorted end-loop. The loop is placed such that the antenna currents flow in the azimuthal direction. The couplers are made entirely from high purity Nb, which is etched, baked and high-pressure water rinsed, such as a superconducting RF cavity. The input and output couplers use the same design. While the input coupler is pushed further into the cavity to achieve a high Q_{ext} , the output coupler is retracted by ~20 mm. Also the coupler needs to be variable (~1" stroke) to allow tuning for the optimum coupling coefficient. A simple scaling from the TESLA input coupler, which was designed for 300 kW and tested for up to 1 MW of pulse power indicates that the coupler design discussed below, would be driven at the edge of its range. With an OD of 9 mm (TESLA: 40 mm), this coupler should be able to carry up to 50 kW of the peak power of the TESLA conductor, approximately what is needed for fast filling. The coupler OD, however, is limited by the space available in the cavity beam tube and on the cryostat bottom flange.

Fig. 25 shows a sketch of a possible coaxial input coupler design. It consists of a 9 mm OD (2 mm wall) Nb tube with a 2 mm diameter Nb rod in the center. The center-rod forms a 5 mm x 5 mm rectangular loop at the end where it is welded to the outer tube. The Nb end-loop is formed and welded to the center pin of the Nb-ceramic-Nb spacer disc. A short piece of Nb outer conductor tube is also welded to the spacer disc to complete the coupler end. Then the center-conductor and outer tube are welded to the end piece. Note that the ceramic-Nb connector needs to be welded to the center conductor before the outer tube is assembled. The coupler is attached to the (cleaned) bellows and the coupler assembly is mounted into the bottom adaptor flange. The coupler passes through a hole in the bottom adaptor flange entering the cavity from below. A sliding contact, made from Nb foil, is attached to inside face of the bottom adaptor flange (see Fig. 4). It masks the gap between the coupler outer conductor and the ID of the hole in the flange. The center conductor is placed at 57 mm from the cavity center axis. In the design shown in Fig. 3 the coupler loop reaches to a distance of 110 mm from the center. The coupler simulations presented in Fig. 11 were performed for cases of a 90 mm and a 100 mm distance, thus for designs in which the coupler is pushed further into the cavity to increase Q_{ext} .

At the end of the coupler outside the cavity the center and outer conductors are welded into a ceramic window flange, which forms the transition to the external

Conceptual Design of a Small Sample High Field RF Test Station

power lines. In the case of the output coupler the power is routed to the RF system via a flexible coaxial line (low power). The input coupler is supplied by a waveguide, low transmission loss. A coax-to-waveguide transfer piece, not shown here, is required in that case. A mechanical adaptor connects the end of the coupler to the horizontal arm of the drive system. Between the outside of the bottom adaptor flange and the coupler end is a bellows section. The bellows gives the coupler 1" of travel. Ideally it is made from hydroformed Nb. The sliding contacts shield the bellows section from fields and therefore stainless maybe also be chosen as material for the bellows. The bellows are attached to the bottom adaptor flange and the RF adaptor via bolted UHV flanges. The couplers are cooled indirectly through the adaptor flange and the bellows.

The coupler drive system consists of a "rocking-chair" mechanism, in which a vertical G10 rod controlled with a step-cantilever bar, which can pivot around its center point where it is affixed to the host cavity cryostat. When pulling on the G10

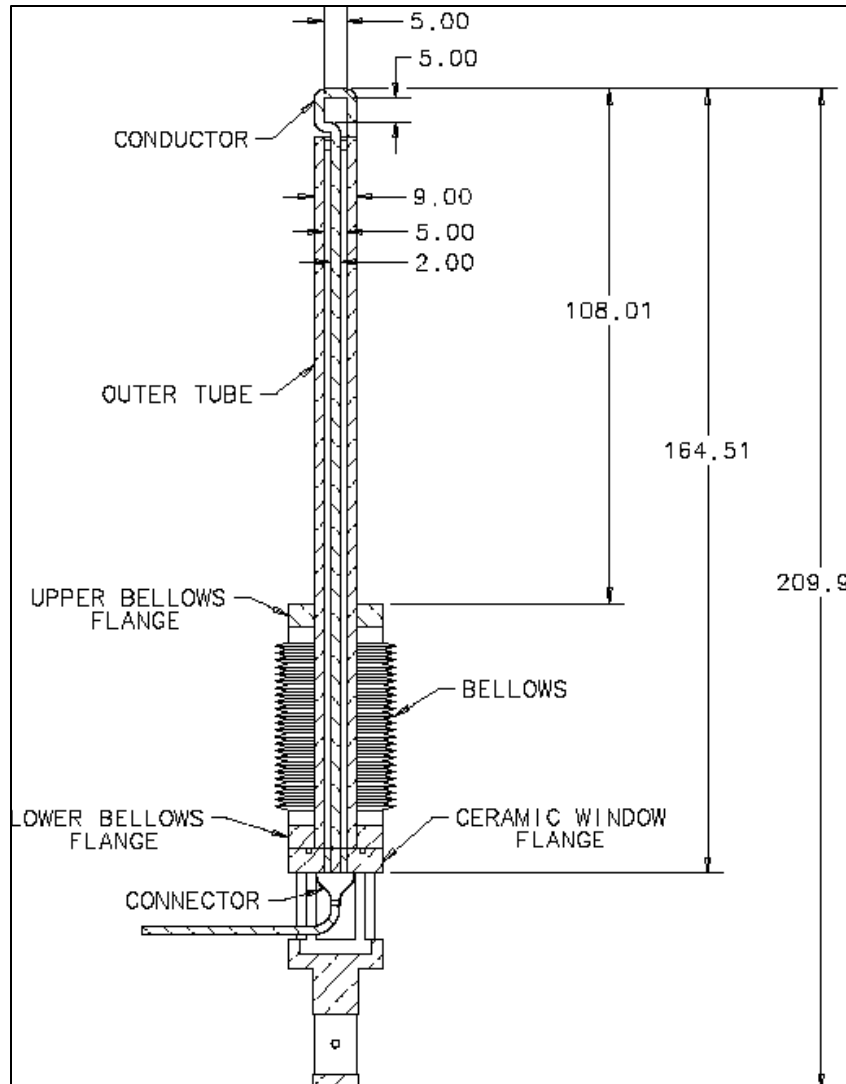


Figure 25: Design of the variable output coupler (all measures in mm).

rod, the coupler is retracted from the cavity. The couplings between the vertical rod, the cantilever as well as between the cantilever and the coupler are such that only vertical motion is transmitted to the coupler. Also a guide plate, which can be seen in Fig. 19 ensures that the coupler cannot be tilted by the coupler drive system's action.

12) RADIATION SHIELDING

In the TE010 mode the electrons are accelerated horizontally, which in the case that the test station is assembled into a pit should not generate any problem. Assuming occasional tests of the host cavity system in the accelerating mode, however, the worst case integrated voltage of ~ 5 MV can be generated in the small sample, high field RF test station. This requires special radiation shielding and monitoring measures that go beyond installing the station in a pit. The radiation shielding needs to attain the goal of keeping the radiation levels to less than 0.1 mrem/hr.

The vertical cavity test stations at TJNAF, in which multi-cell cavities for CEBAF and SNS are being tested, were chosen as model for the radiation mitigation strategies for this system, although the cavities tested there typically generate larger integrated voltages than in the case discussed here.

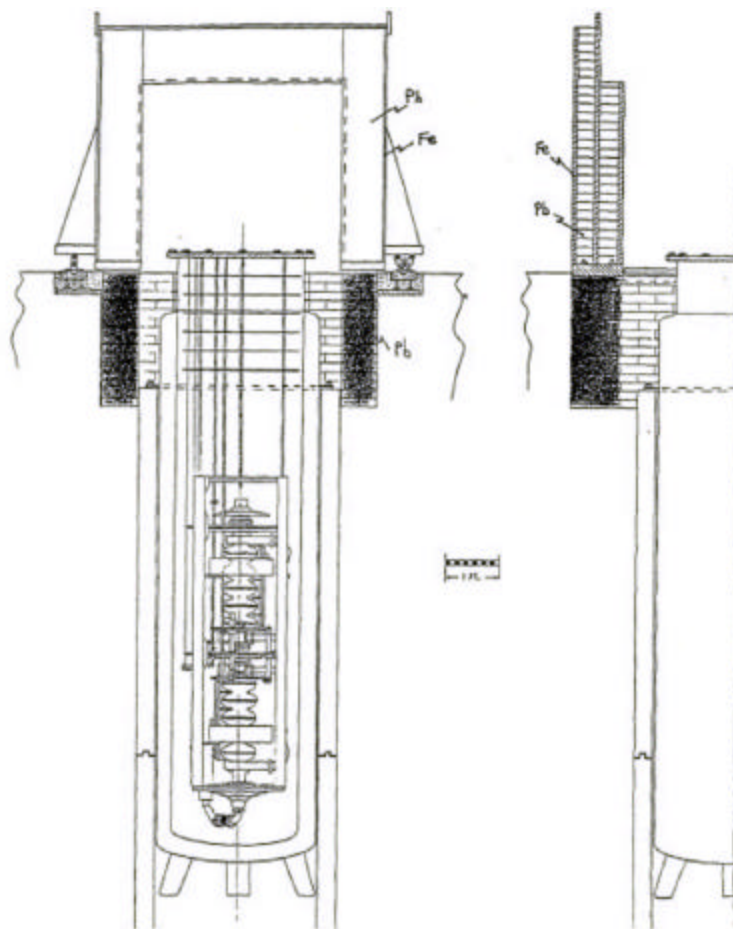


Figure 26: Radiation shield of vertical cavity test station at TJNAF.

At TJNAF the test stations are placed in pits. The shielding consists of 5-sided boxes that cover the test station top plate, also extending ~ 0.5 m into the pit (Fig. 26). The boxes consist of steel frames holding 8" thick lead plates. Radiation monitors inside and outside (at 6-12 m from Dewars) the shield lids monitor gamma production and possible radiation leakage around the penetrations of the shield (for cryo-lines, etc). At TJNAF the radiation levels within the shield can be as high as 80 R/hr. Outside the shields

levels are typically 1-5 mR/hr on contact and 0.1-0.5 mR/hr (whole body dose) at 30 cm. Therefore the TJNAF shield design is appropriate for the purpose of the small sample high field superconducting RF test station.

13) STEP-BY-STEP APPROACH

The small sample, high field RF station is a challenging device. Before engaging in the construction of this highly complex system it should be clarified if it is possible to achieve high Q in a host cavity with a central Nb rod. The sapphire tube also needs to be tested in a separate test to assess to which level heating and field emission can be reduced. The following describes different pre-cursor experiments that are needed to determine if the proposed technical solutions work and, in some specific cases, to test different solutions that could lead to cost reduction or more simplicity.

- 1) Experiments at DESY have shown that TESLA single cell cavities could be operated in the TE010 mode at $Q=2 \times 10^{10}$ up to ~120 mT peak fields. This is still short of the record magnetic surface fields reached in TESLA single cell cavities in the accelerating mode (~180 mT). It is hoped that DESY will soon be able to pursue these tests and reach even higher fields in the TE010 mode.
- 2) As a first test (conducted for example in the existing vertical cryostat at A0) a Nb cavity, either the future host cavity or some other, should be tested with and without a Nb rod in the center. The Nb rod can be assembled into the flanges that close up the cavity at both extremities. As an additional experiment the Nb-tube can be hollow in one case such that it is cooled from the inside by the superfluid helium that also cools the cavity. To perform this measurement in the TE010 mode, however, couplers such as described in chapter 12 are needed. The fabrication of such couplers represents a significant effort. As an extension of this experiment the sapphire bore can be assembled into the host cavity as well to test its behavior at high RF fields.
- 3) Once the rod-in-cavity principle and the use of the sapphire bore are established the host cavity should be assembled. Bench measurements using e.g. bead-pulls have to be performed to make sure that the expected field profile and mode spectrum is obtained.

Should it turn out that, as a result of field emission, RF heating or some other reason, the sapphire bore cannot be implemented, the design presented here can also be made to work without it. The price to pay, however, is in more stringent procedural requirements for the cleanliness of the sample exchange process, possibly forcing operation of the test facility in a clean room environment.

Some ideas were brought forward that could result in the elimination of the high power klystron, the cost driver in this facility:

- One option would be to cool the RF dissipation on the sample with superfluid helium directly on RF exposed surface. This would require a different cryo-design in which the sapphire bore contains superfluid helium and protects the host cavity from it. Most importantly, a test that shows that liquid helium can be exposed to strong RF fields is needed.

- The use of a lower frequency cavity (~600 MHz) could allow to operate the TE010 mode at ~1.3 GHz, thus leading to a reduction of the surface heating. One option is the fabrication of a new specially made host cavity. Another option is to use e.g. an SNS 800 MHz single cell cavity and adapt it to this purpose (since the SNS cavities are for low β , stretching of the cavity would be required).

14) COST ESTIMATE

The following approximate cost estimate includes only M&S expenses for a RF materials test facility such as described in this document. No design, machining or assembly labor is included. It does not include contingency and can only be considered a rough indicator of the final cost of the facility. Not included in this estimate is the cost of large cold pumps for the 2 K cryo-system and the source of LHe (Dewars or liquefier). This hardware exists at the development and test facility at Fermilab. Also not included is the cost of a pit and a klystron gallery.

Table 4: Cost estimate for components of the small sample, high field RF test station.

	Qu	Cost/ unit (k\$)	Comment
Host cavity	1	-	single cell cavity, TESLA type w/ flanges - DESY
2.635 GHz Klystron	1	190	50 kW, CPI – Toshiba, price quoted from 3 rd harmonic klystron; incl. modulator
Variable couplers	2	25	Coupler, feed-throughs, bellows, flanges, guide-flanges, ceramic, incl. welding and cleaning, input and output, drive system, no development cost incl.
Cryostat	1	37	1.5 m ³ volume, LN and LHe shields, budgetary estimate by CRYOFAB, Ma
Host cavity cryostat	1	29	Nitronic 40, incl. bellows, feed-through for diagnostics, and welding, NbTi top adaptor flange (5 k\$), NbTi bottom adaptor flange (8 k\$), cold finger (3 k\$), diagnostics (5 k\$)
Vacuum	1	28	Pumping station for host cavity (5 k\$), UHV gate valve (5 k\$), sample vacuum vessel incl. bellows (5 k\$), vacuum diagnostics sample (3 k\$), load-lock RGA (10 k\$)

Conceptual Design of a Small Sample High Field RF Test Station

TWTA – RF amplifier	1	25	Varion V2C6963G1D, catalogue item
RF system	1	25	2 power meters HP E44198 (a 5 k\$ each), 1 scope TEK-TDS-380 (a 5 k\$), 2 circulators MW A3654 (a 0.5 k\$), directional coupler NARDA 503A-03 (0.5 k\$), 1 Trombone-phase shifter (1 k\$), 2 diode detectors (a 1 k\$ each), 1 amplifier (a 2 k\$), phase detector, DC blockers, cables,..etc
2 K Cryo-system	1	25	5 K vessel incl. plumbing (5 k\$), heat exchanger (2 k\$), JT valve assembly (2 k\$), 2K pumping line incl. bellows (5 k\$), diagnostics (5 k\$), 90 K and 5 K pre-cooler stages for sample (2 k\$), pumping station (5 k\$)
Sample transfer system	1	20	UHV compatible x,y,z sample transfer stage, Omniax, quote from Advent Associates, II
Sapphire bore	2	10	single-crystal tube (35 mm OD, 1 mm wall), one tube reserve, Bigstone, catalogue item
Top radiation shield	1	18	8" lead bricks, stainless frame, hydraulic, radiation diagnostics (3 k\$)
Insert - mechanical	1	15	Frame, cross-bars, support rods, incl. MLI, 2 SS baffles, 2 Cu shields with LN spiral and plumbing
Magnetic shield	1	10	Perm-alloy (Amuneal, Pa, 100\$/sqft), 2 layers, Al frame, incl. re-annealing,
Load-lock chamber	1	10	UHV chamber with access ports, windows for visibility, heaters for outgassing, Advent Associates, II
Rs measurement		7	6 calibrated Cernox temperature sensors (5 k\$), 2 tape heaters, DVMs (2 k\$),
Control system		4	PC (3 k\$), racks (1 k\$), Labview - program based
Total		513	In house labor for design, assembly, testing and fabrication not included;

APPENDIX A

Formulas used in the thermal model calculations:

The BCS surface resistance is calculated according to H. Padamsee⁵ [p. 88].

$$R_{s,BCS}(T, f) = 1.7 \frac{2 \cdot 10^{-4}}{T(K)} \left(\frac{f(GHz)}{1.5} \right)^2 e^{\frac{17.67}{T(K)}} \quad (\Omega) \quad (A-1)$$

At the operating parameters of $f_0 = 2.635$ GHz and $T_{b0} = 2$ K the BCS surface resistance in Nb is ~ 75 n Ω .

The thermal conductivity of Nb according to the Koechlin-Benin model⁶ uses modified constants to calibrate a theoretically accurate model to measurement data. The total thermal conductivity is a sum of the electron and phonon contributions, $k_{el} + k_{phon}$.

The electron contribution is regulated by the number of electrons at the Fermi-level, which are not condensed into the superconducting phase. A polynomial fit of the normalized superconducting electron function is:

$$R(y) = 10^{-4} y^4 - 5.4 \cdot 10^{-3} y^3 + 0.1017 y^2 - 0.7848 y + 2.1282 \quad a' < y < 8 \quad R(y > 8) = 1 \quad (A-2)$$

The electronic contributions to the thermal conductivity are given with Wiedemann-Franz ($L' = 2.11 \times 10^{-8} \text{ W}\Omega/\text{K}^2$) and electron-phonon exchange ($F_{el-phon} = 7.6 \times 10^{-7} \text{ m/W/K}$). Note that the argument of the superconducting electron function is $\alpha' T_c / T$, with $\alpha' = 1.53$, the modified BCS gap parameter.

$$k_{el}(T, RRR) = R \left(a' \frac{T_c}{T} \right) \frac{1}{\left(\frac{r(295K)}{L' RRR T} \right) + F_{el-phon} T^2} \quad \left(\frac{W}{K-m} \right) \quad (A-3)$$

The phonon contribution is given with the phonon-electron scattering contribution $C_1 = 234 \text{ mK}^3/\text{W}$ and the scattering at the grain-boundaries $C_2 = 4.34 \times 10^3 \text{ W/K}^4/\text{m}^2$. The phonon mean free path $l_{mfp,phon}$ here is assumed to be the grain size.

$$k_{phon}(T) = \frac{(1 + f_{peak})}{C_1 T^{-2} e^{-a' \frac{T_c}{T}} + \frac{1}{C_2 l_{mfp,phon} T^3}} \quad \left(\frac{W}{K-m} \right) \quad (A-4)$$

⁵ H. Padamsee, J. Knobloch, T. Hays "RF Superconductivity for Accelerators", J. Wiley & Sons, New York, 1998

⁶ F. Koechlin, B. Benin, "Parametrisation of the Niobium Thermal Conductivity in the Superconducting State", CEA internal note DAPNIA-SEA-96-01, Jan. 1996

To be conservative the phonon-peak at ~ 2 K was kept very modest in this calculation ($f_{peak,max}=1$).

A phenomenological fit for the Kapitza conductance for $T-T_b < 1.4$ K was proposed by Mittag⁷.

$$a_{Kap}(T) = 200 \cdot (T_b^{4.65}) \left[1 + 1.5 \left(\frac{T-T_b}{T_b} \right) + \left(\frac{T-T_b}{T_b} \right)^2 + 0.25 \left(\frac{T-T_b}{T_b} \right)^3 \right] \left(\frac{W}{Km^2} \right) \quad (A-5)$$

In addition the condition was introduced that at a normalized heat flux $p > 10$ kW/m², the Kapitza conductance is replaced by $a_{FB}=250$ W/m²/K, the film-boiling heat transfer coefficient to take into account the onset of boil-off.

The temperature profile across the Nb sheet of thickness d (including Kapitza impedance at Nb-He interface and transition to film-boiling at $P > 10$ kW/m²) was calculated according to the following procedure:

The temperature profile across the Nb sheet (thickness w , number of elements N , element thickness D) between the outer surface cooled by superfluid helium to the inside surface exposed to RF fields is calculated iteratively from a start ("guess") value for the temperature at the inside surface. The temperature in segment i of thickness D (counting starts at the bath side where $T_0=T_{b0}$) is calculated with equation (A-6) from the RF power calculated from the guess value for the RF surface temperature T_{guess} and the peak field. The RF dissipation is calculated from the temperature dependent BCS surface resistance (to which a fixed residual resistance is added) in (A-1) and the peak field H_{peak} ($p_{RF}=R_s H_{peak}^2$). The local temperature within segment i is taken into account when calculating the local thermal conductivity k ((A-3)+(A-4)). The temperature step due to the Kapitza resistance (conductance a_{Kap}) at the Nb-He interface is also taken into account in the calculation of the first value of the temperature array.

$$i=1 \quad T_1 = T_{b0} + \frac{p_{RF}(T_{guess}, H_{peak}, \dots)}{a_{Kap}}, \quad i > 1 \quad T_i = T_{i-1} + \frac{p_{RF}(T_{guess}, H_{peak}, \dots) \Delta}{k(T_{i-1})} \quad (A-6)$$

The temperature at the RF surface is the last value in the T_i array, T_N . This temperature becomes the new guess (start) temperature for a subsequent iteration until expression (A-7) is smaller than some upper threshold. When $T_N=T_{guess}$, a self-consistent set of temperatures is found and the RF heat flux generated on the inside surface becomes equal to the heat flux across the Nb wall.

$$e = \left| \frac{k \left(\frac{T_{guess} - T_{b0}}{2} \right) w}{1m^2} (T_{guess} - T_{b0} - \Delta T_{Kap}) - p_{RF}(T_{guess}) \right| \left(\frac{W}{m^2} \right) \quad (A-7)$$

⁷ Cryogenics, Vol. 13, p. 94, 1973

The above formalism allows calculation of the equilibrium temperature distribution across the cavity or sample wall for a steady RF surface power deposition. To calculate the surface temperature during short RF pulses a pseudo-transient model was developed. This model derives the temperature rise using a linearized heat balance equation (A-8):

$$\Delta T(T, H) = \frac{p_{RF}(T, H)}{w \left[\frac{c_p(\bar{T})}{\Delta t} + \frac{k(RRR, \bar{T})}{A} \right]} ; \quad T_k = T_{k-1} + \Delta T(T_{k-1}, H) \quad (\text{A-8})$$

The temperature rise on the RF exposed surface during the short interval Δt is calculated from the amount of heat $p_{RF} \Delta t$ deposited during that interval. This, of course, assumes that the pulse rise time is infinitely short. This infinitesimal heat increment is partly conducted out of the Nb wall with thickness w (typically several mm) with the conductivity k (neglecting the Kapitza contribution to the thermal impedance and assuming that no burn-out occurs at the Nb-He interface) and partly absorbed by the Nb enthalpy (c_p). The material properties k and c_p are calculated at an average temperature $T_{av} = (T_{surface} + T_b)/2$. The evolution of the surface temperature in time is calculated iteratively by adding the instantaneous ΔT calculated in this way. The pseudo transient model is valid only for the condition that the thermal diffusion time is shorter than the pulse time. At 2 K the diffusion time in Nb as calculated from k and c_p (see below) is ~ 1 msec, close to the pulse-times of interest.

The temperature dependent specific heat function used in the transient model is given with (A-9) and the density of Nb $\rho = 8570 \text{ kg/m}^3$ and the specific heat of Nb at room temperature $cp_{Nb, 300K} = 2.27 \text{ MJ/K/m}^3$:

$$cp_{Nb, low}(T) = 0.085 \frac{J}{K^2 kg} \rho_{Nb} T + 0.00012 \frac{J}{K^4 kg} \rho_{Nb} T^3 \left(\frac{J}{Km^3} \right)$$

$$cp_{Nb}(T) = \frac{1}{\left(\frac{1}{cp_{Nb, 300K}} \right) + \left(\frac{1}{cp_{Nb, low}(T)} \right)} \left(\frac{J}{Km^3} \right) \quad (\text{A-9})$$

APPENDIX B

The formulas used in the Dewar design heat load calculations were mostly taken from Darve⁸.

The heat conduction through a structural element of cross-sectional area A and length L with temperatures T_1 and T_2 at the ends ($T_1 > T_2$) is calculated with:

$$Q_{cond} = \frac{A}{L} \int_{T_2}^{T_1} k(T') dT' \quad (W) \quad (B-1)$$

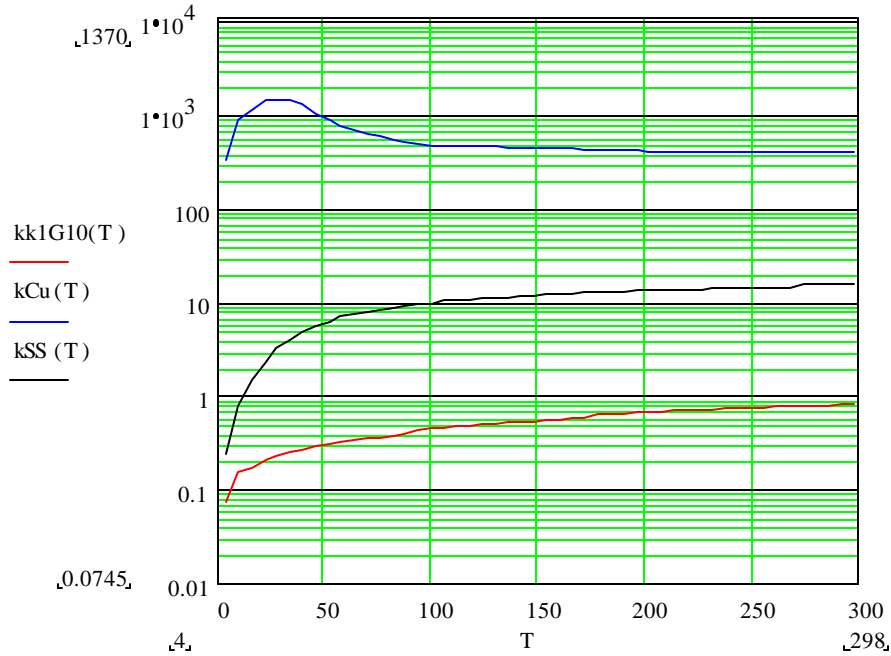
from its thermal conductivity $k(T)$.

Using a fit of experimental data obtained from the CTM2 experiment at Cern, the radiation heat load emitted by an outer cylinder at temperature T_1 deposited onto the inner cylinder with surface A and at temperature T_2 (as well as protected by N layers of MLI and at a vacuum pressure of 10^{-6} mbar) is given with:

$$Q_{cond} = A \left[\frac{1.4 \cdot 10^{-4}}{N} \left(\frac{T_1^2 - T_2^2}{2} \right) + \frac{3.74 \cdot 10^{-9}}{N} (T_1^2 - T_2^2) \right] \quad (W) \quad (B-2)$$

The fit (B-2) is valid only for materials with an emissivity similar to that of stainless steel (0.1 at 4 K, 0.2 at 300 K).

The temperature dependent thermal conductivity (in W/K/m) of stainless steel, copper and G10 used in the Dewar thermal model calculations is given in the plot below:



⁸ C. Darve et al., "Thermal Performance Measurements on a 10 m long Dipole Prototype Cryostat (Cryostat Thermal Model 2)", LHC project note 112, CERN, Nov. 1997

APPENDIX C

Assumptions and equations used in the temperature drop analysis through superfluid:

1. Heat transport through the pressurized superfluid with constant cross-section and

constant heat flux obeys $\frac{dT}{dx} = f(T)q^m$ where $m = 3$ and q is the heat flux in W/cm^2 (Van Sciver, "Helium Cryogenics", pp. 143 - 144). If from 1.85 K to 1.95 K, we assume $f(T)$ is constant, and $\frac{1}{f(T)} = 1200$, then $\Delta T = \frac{q^3 L}{1200}$ where L is

distance in cm, q is the heat flux in W/cm^2 , and ΔT is the temperature difference through the conduit in Kelvin.

2. For a constant wall heat flux within a tube, assume the heat flux through the pressurized superfluid increases linearly with position (constant wall heat flux),

and again assume $\frac{1}{f(T)} = \text{const}$. One may then easily integrate $\frac{dT}{dx} = f(T)q^m$

over the length of the tube, where $q = q_0 + \frac{Qx}{A}$, q_0 is the heat flux through the

superfluid into the system, Q is the heat added per unit length (e.g., W/m), A is the heat flow passage area, and x is distance along the heat flow passage. Substituting and rearranging results in the following integration:

$$\int \frac{dT}{f(T)} = \int \left(q_0 + \frac{Qx}{A} \right)^m dx. \text{ With } f(T), q_0, Q, \text{ and } A \text{ all constant, integrating from}$$

$$x=0 \text{ to } x=L \text{ gives } \Delta T = \frac{A}{(m+1)Q(1/f(T))} \left\{ \left(q_0 + \frac{QL}{A} \right)^{m+1} - q_0^{m+1} \right\}. \text{ Note that}$$

$$q_0 + \frac{QL}{A} = q_L \text{ where } q_L \text{ is the heat flux at the } x=L \text{ end of the heat flow passage.}$$

Thus, the temperature difference through the passage may be written as

$$\Delta T = \frac{A}{(m+1)Q(1/f(T))} (q_L^{m+1} - q_0^{m+1}).$$

For calculations of non-uniform heat flux, short segments of uniform heat flux are added, and the equation in (2) above is used.

3. For a given temperature the saturated vapor pressure is calculated with Clausius Clapeyron. For further simplification the calculation is performed on the basis of

a reference value of 0.031 atm at 2 K: $p_{SVP}(T) = p_{SVP}(2K) e^{\frac{1}{R_{He}}(\frac{1}{T_2} - \frac{1}{T})}$, where the latent heat $\lambda = 23.4$ J/g and $R_{He} = 2.078$ J/g/K. The liquid overhead d (cm) needed to provide the hydrostatic pressure to overcome the saturation vapor pressure

$$\Delta p(\text{atm}) \text{ is: } d = \frac{\Delta p \times 1.013 \cdot 10^6}{0.146 \cdot 980.7}$$